United States
Environmental Protection
Agency

Office of Research and
Development
Washington DC 20460

EPA/600/R-96/079
July 1996

EPA

Prehatching Development of the Fathead Minnow *Pimephales Promelas* Rafinesque

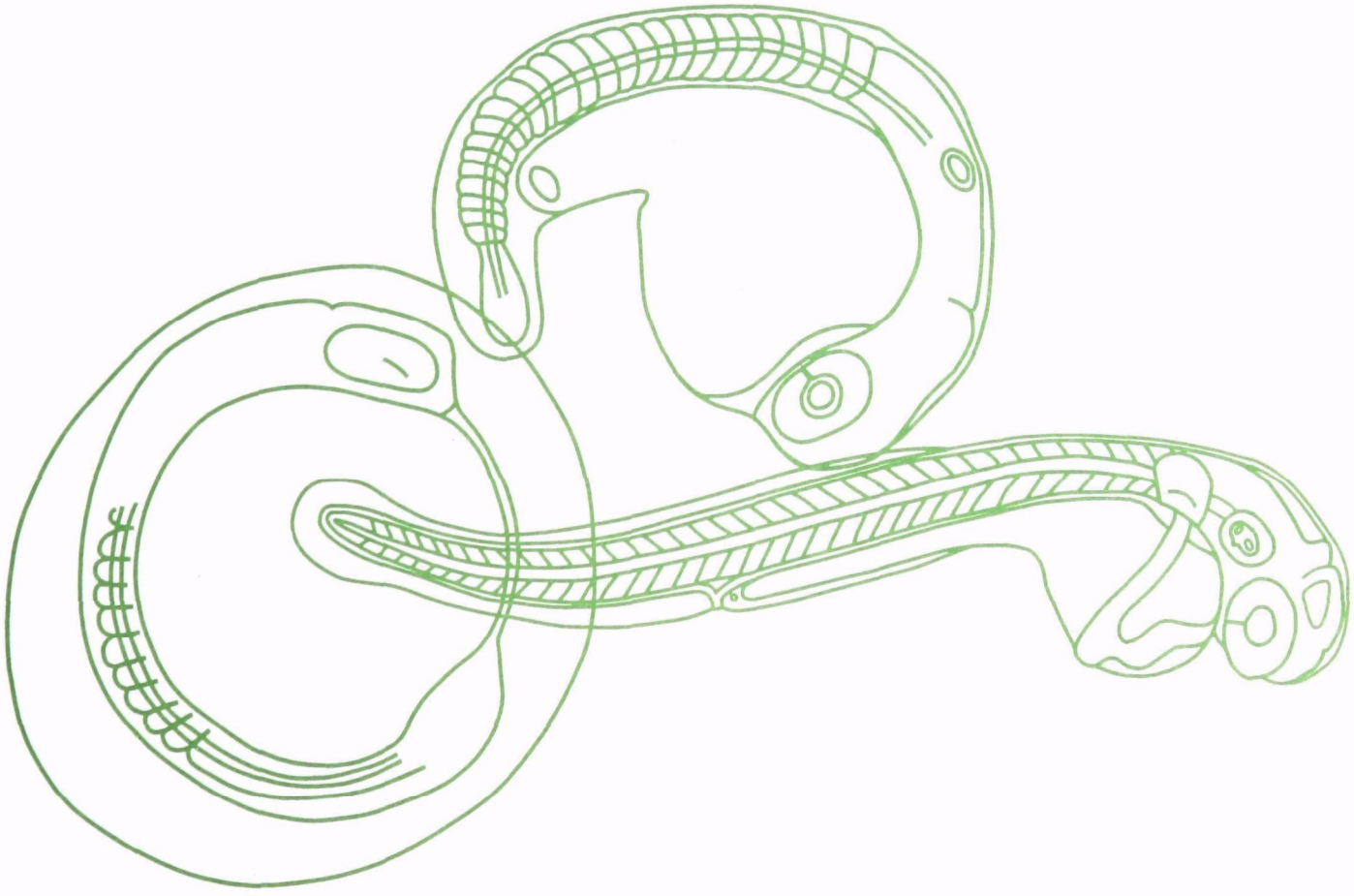

EPA/600/R-96/079
July 1996

PREHATCHING DEVELOPMENT OF THE FATHEAD MINNOW *PIMEPHALES PROMELAS* RAFINESQUE

By

E. W. Devlin,[1] J. D. Brammer,[2] R. L. Puyear,[2] and J. M. McKim[3]

[1]Biology Department, Hampden-Sydney College, Hampden-Sydney VA
[2]Zoology Department, North Dakota State University, Fargo, ND 58105
[3]USEPA, Mid-Continent Ecology Division, Duluth, MN 55804

U.S. ENVIRONMENTAL PROTECTION AGENCY
OFFICE OF RESEARCH AND DEVELOPMENT
NATIONAL HEALTH AND ENVIRONMENTAL EFFECTS RESEARCH LABORATORY

NOTICE

This document has been reviewed in accordance with U.S. Environmental Protection Agency policy and approved for publication. Mention of trade names or commercial products does not constitute endorsement or recommendation for use.

ABSTRACT

The fathead minnow, *Pimephales promelas* Raf., presents a classical model of teleostean embryogenesis. Its prehatching development has been divided into 32 stages, each representing an easily observed interval in the developmental continuum. Embryos were examined live and histologically under controlled laboratory conditions. Fertilization, early cleavage, epiboly, and organogenesis are very similar to that of other cyprinids except for the timing of the appearance of specific structures. Hatching was found to occur in approximately 120 hours post-fertilization at 25°C. Rapid embryonic development, coupled with a short generation time of 3-6 months under laboratory conditions, make it a useful native North American species for studies in experimental embryology.

TABLE OF CONTENTS

LIST OF TABLES

Number **Page**

LIST OF PLATES

GLOSSARY

3v	Third ventricle
4v	Fourth ventricle
A	Anterior
AA	Aortic arches
B	Blastomere
BD	Bile duct
Bl	Blastoderm
C	Chorion
Ca	Caudal
CA	Caudal artery
cc	Common cardinals
CF	Choroid fissure
ChP	Choroid plexus
CK	Caudal knob
Cl	Cloaca
ClF	Cleavage furrow
Co	Coelomic cavity
CPl	Cleavage planes
CV	Caudal vein
Cy	Cytoplasm
D	Diencephalon
DT	Dorsal tube
EE	Epidermal ectoderm
EmS	Embryonic shield
Ep	Epiphysis
ES	Epidermal stratum
Fg	Foregut
G	Gut
GA	Gill arches
GB	Gallbladder
GL	Ganglion cell layer
GR	Germ ring
H	Heart
HA	Heart anlage
HE	Head ectoderm
HR	Head region
HV	Heart ventricle
I	Infundibulum
INL	Inner nuclear layer
IPL	Internal plexiform layer
KV	Kupffer's vesicle
L	Lens
LD	Line drawing
LDi	Liver diverticulum
Li	Liver
LiS	Liver sinusoids
LJ	Lower jaw
LP	Lens placode
LS	Live specimen
M	Micropyle
Mc	Melanocytes
Me	Mesencephalon
MF	Mesen-metencephalon fissure
MFF	Median fin fold
Mt	Mitotic figures
Mv	Microvilli
N	Notochord
Nc	Neurocoele
NC	Nerve Cord
NCr	Neural crest cells
Nk	Neural keel
Nm	Neuromeres
Nmt	Neuromast
Nu	Nucleus
O	Otoliths
OA	Optic anlage
OC	Optic cup
OG	Olfactory groove
OlP	Olfactory placode
ON	Optic Nerve
ONL	Outer nuclear layer
Op	Operculum
Otc	Otic capsule
OtP	Otic placode
OtV	Otic vesicle
OV	Optic vesicle
P	Periblast
PC	Periblast corona
PCo	Pericardial coelom
PD	Pronephric ducts
PF	Pectoral fin
Ph	Pharynx
PN	Periblast nuclei
Pr	Prosencephalon
PS	Paraffin section
Pt	Proctodeum
PT	Pronephric tubule
PvS	Perivitelline space
R	Rhombencephalon
RC	Radial cartilage
S	Somite
HS	Hyaline sheath
SA	Somite anlage
SB	Swim bladder
Sc	Sclerotic coat
SC	Spinal cord
SEM	Scanning electron microscope
Sg	Segmentation cavity
SM	Segmental mesoderm
St	Stomach
StC	Striated cartilage
T	Telencephalon
TB	Tailbud
TL	Tectal lobe
TP	Thickened periblast
V	Unlined vesicle
WM	White matter
Y	Yolk (mass)
YlP	Yolk plug
YP	Yolk particles

ACKNOWLEDGEMENTS

We wish to thank Dr. Conrad Firling, University of Minnesota, Duluth and Dr. Rodney Johnson, Environmental Research Laboratory, Duluth for their review and comments on the Manuscript. Finally, this research was partially funded by Air Force Research Grant AFOSR-78-3709, and National Institutes of Health Environmental Pathology Training Grant 5T32ES07032.

INTRODUCTION

The use of fish embryos as models to study the action of toxic substances has been going on since the early 1900's with the work of Stockard (1910), McClendon (1912), and others. These workers recognized their utility as model organisms, offering many advantages over mammalian systems: the embryo is contained within a chorion which is often clear allowing observation of embryogenesis without perturbation of the embryo; teleost embryos are often easily cultured in the lab year-round; many species offer large numbers of eggs from one female (minimizing much of the variability when using gametes from many individuals), depending on the species chosen, a large range of developmental rates are available (Table 1).

Different teleostean species exhibit a range of developmental complexity at hatching. This is seen in the developmental stage of the musculature, integument and skeletal or the extent of yolk utilization. For example, in the slower developing salmonids the newly hatched larvae possess a large yolk sac which results in limited mobility. At hatching the fathead minnow, *Pimephales promelas*, is well developed possessing a streamlined yolk sac, partial body pigmentation, an open mouth with movable jaws, well developed musculature, eyes and neuromasts system (as evidenced by attempts to catch the newly hatched larvae) and is able to feed shortly following hatching. It should be noted that this post-hatch period between complete utilization of yolk stores and exogenous feeding represents a time of metabolic stress in which the young larvae are especially vulnerable to stress (Devlin, 1982). The present study has concentrated on development up to hatching, further work on the later larval stages would also be useful.

The fathead minnow is a small hardy cyprinid that is an important forage fish (Lord, 1927). Its life cycle has been described by Markaus (1934), Bullough (1939), Andrews (1970), and Andrews and Flickinger (1974). The relatively simple procedure for obtaining fathead minnow eggs, as well as its short generation time of 3 to 6 months under controlled conditions, has made it useful in toxicological studies (Benoit and Carlson, 1977; McKim, 1977; Till, 1977). Yet in spite of its ecological significance and widespread use in laboratory studies, descriptions of its early development are incomplete. Partial descriptions of its embryonic development have been reported (Niazi, 1963; Manner and DeWese, 1974; Wabuke-Bunoti, 1980).

These descriptions are useful, but do not allow investigators to accurately assign a stage of development, nor do they provide a complete detailed description of normal development.

Many accounts of teleost embryogenesis are available (Table 1). In reviewing this literature, the timing of appearance of embryonic structures is seen to differ among teleosts. Indeed, although generalized patterns of development exist, there is enough variation to make any standard staging sequence beyond the limits of the suborder unreliable (Long and Ballard, 1976). The present study provides a detailed embryonic staging sequence, which will allow a more widespread use of the fathead minnow as a model organism in laboratory studies.

Table 1. Selected species whose embryonic development has been described.

Species	Age at Hatch (hrs)	Temp (°C)	Number of Stages	Author
Abudefduf saxatilis	158*	24	19	Shaw, 1955
Adinia xenica	239*	27	33	Koenig & Livingston, 1976
Austrofundulus myersi	1248	25	46	Wourms, 1972
Barbus barbus	194	16	7	Penaz, 1973
Brachydanio rerio	96	26	25	Hisaoka & Battle, 1958
Carassius auratus	100	21	25	Kajishima, 1960
Catostomus commersoni	492*	10	22	Long & Ballard, 1976
Coregonus clupeaformis	3120	10	803	Price, 1934; Price, 1935
Erimyzon sucetta	106*	21	21	Shaklee et al., 1974
Esox masquinongy	336	13	--	Galat, 1973
Fundulus heteroclitus	228	20	34	Armstrong & Child, 1965
Gasterosteus aculeatus	140	17	--	Vrat, 1949
Heteropneustes fossilis	7*	28	--	Thakur et al., 1974
Ictalurus punctatus	--	26	19	Saksena et al., 1961
Macropodus opercularis	36	27	--	Allen & Mulkay, 1960
Micromesistius poutassou	20	8	4	Coombs & Hiby, 1979
Micropterus dolomieui	44*	23	16	Wallace, 1972
Myoxocephalus aenaeus	1008*	6	--	Lund & March, 1975
Notropis bifrenatus	57	26	15	Harrington, 1947
Oncorhynchus kisutch	960	10	--	Zeitoun, 1974
Oncorhynchus keta	--	8	16	Mahon & Hoar, 1956
Oncorhynchus nerka	1170	10	30	Velsen, 1980
Oryzias latipes	264	25	36	Kirchen & West, 1976
Perca flavescens	848	10	8	Mansueti, 1964
Pimephales promelas	--	23	12	Manner & Dewese, 1974
Polyodon spathula	240	14	36	Ballard & Needham, 1964
Pomatomus saltatrix	47*	20	--	Deuel et al., 1966
Pseudopleuronectes americanus	360	2	--	Breder, 1922
Salmo gairdneri	600	10	23	Ballard 1973
Salmo solar	4444*	1	34	Battle, 1944
Serranus atrarius	75	16	--	Wilson, 1891
Tilapia galilae	48	24	4	El Zarka & Ezzat, 1972
Trichogaster trichopterus	23*	26	--	Hodges & Behre, 1953

* Midrange of the reported range of values

METHODS AND MATERIALS

Fathead minnows were obtained from stock cultures at the U.S. Environmental Research Laboratory, Duluth, MN (Denny, 1987). Breeding facilities in our laboratory consisted of 28 10-liter tanks, each containing a U-shaped tile, one mature male, and two mature females. All tanks were fitted with standpipes and individually supplied with air and water. City water (pH 8.3, hardness 80 mg/l CaCO3) passed through activated carbon was used in all tanks. Water temperature was maintained at 24°C±0.5. The whole culture system was enclosed in a light-tight insulated room, with a photoperiod of 16 hr light (100 lux at the water surface) and 8 hr dark. Mature fish were fed frozen brine shrimp and Glenco No. 2 enriched trout food twice daily. Larval fish were fed brine shrimp twice daily.

In order to observe events at fertilization, mature ova were obtained by removal of fully developed ovaries from gravid females and added to sperm suspensions obtained from mature minced testis. To observe later stages, embryos were removed from the underside of the U-shaped tiles in the breeding tanks, placed in aerated 2-liter tanks maintained at 25°C±0.2, and maintained under the same photoperiod (25 lux at the water surface) as the adults. At predetermined intervals, 5 to 10 embryos were gently removed from the tiles for observation.

Embryos for light microscopy were dissected out of their chorion, photographed with a compound microscope, fixed in formalin-acetic acid-alcohol (FAA) (Humason, 1979), embedded in paraffin, serially sectioned at 6 μ and 10 μ, and stained with Harris hematoxylin and eosin. Sections were photographed with a compound microscope. Measurements of average length were determined with an ocular micrometer calibratedin hundredths of a millimeter from a sample of 15 embryos.

Embryos for scanning electron microscopy were fixed in 4% phosphate-buffered glutaraldehyde (pH 7.4) overnight, rinsed three times in buffer, then postfixed in 2% OsO_4 for 3-5 hr. Fixations were carried out at 4°C. Following osmium fixation, embryos were again rinsed in buffer, dehydrated with ethanol at room temperature, and immediately critically point dried with liquid CO_2 in a Samdri PVT-3. Embryos were mounted on stubs and coated with gold in a Hummer II sputter coater. A JOEL JSM-35 scanning electron microscope was used to examine specimens.

RESULTS AND DISCUSSION

This study describes the prehatching development of the fathead minnow under controlled laboratory conditions in which the development is divided into 32 stages (Table 2). In addition, preliminary posthatch descriptions of 9 larval developmental stages were made on this minnow at 25°C (Table 3).

The following detailed fathead minnow prehatching development sequence is described in 32 individual stage descriptions with accompanying photographic plates:

Table 2. Characterization of embryonic stages of *Pimephales promelas* at 25°C.

Dev. Stage	Age (hours)	Length (mm)	Characteristics of the Embryo Stage
1	0.00		Unfertilized ovum
2	0.16		Recently fertilized ovum
3	0.66		1-celled blastodisc
4	1.00		2-celled blastodisc
5	1.33	-	4-celled blastodisc
6	1.58	-	8-celled blastodisc
7	2.25		16-celled blastodisc
8	2.83		32-celled blastodisc
9	3.50		Late cleavage
10	4.50		High blastula
11	5.25		Flat blastula
12	6.00		Early gastrula
13	7.33	-	One-quarter epiboly
14	9.50		One-half epiboly
15	12.00		Three-quarter epiboly
16	15.00		Closure of the germ ring
17	16.50		Neurula stage, 4-5 somite pairs
18	17.75		Optic vesicles, 9-10 somite pairs
19	20.00		Neuromeres, 14 somite pairs
20	22.00		Otic vesicle, 16 somite pairs
21	24.00		Tailbud stage, 18-20 somite pairs
22	26.00		First movements, lens formation
23	30.00	2.19	Heartbeat without circulation
24	35.33	2.83	Onset of circulation
25	40.00	3.35	Retinal pigmentation
26	50.00	3.56	Blood in intersegmental arteries
27	60.00	3.89	Horizontal duct in otic capsule
28	74.00	4.53	Blood flow in pectoral fins
29	85.00	4.90	Formation of yellow bile
30	95.00	5.10	Dorsally pigmented swim bladder
31	105.00	5.18	Large operculum, limited hatching
32	120.00	5.14	Gill anlagen, hatching

Table 3. A preliminary time sequence of the larval stages* of *Pimephales promelas* from hatching through thejuvenile phase of development at a mean water temperature of 25°C.

Dev. Stage	Age in Hours (post-hatch)	Characteristics of Larval Stage
1	12.0	*protolarval phase* (median fin fold)
2	24.0	posterior air bladder filled
3	32.0	yolk-sac disappears
4	56.5	exogenous feeding
5	98.5	*mesolarval phase* (partial fin ray development)
6	223.0	anterior air bladder filled
7	273.0	*metalarval phase* (pelvic fin buds)
8	299.0	caudal fin, symmetrical
9	443.0	*juvenile phase* (fin development complete)

*Approximately 50 larval fish were used to establish these 9 posthatch larval stages.

FATHEAD MINNOW PREHATCHING DEVELOPMENT
PLATES 1 - 32

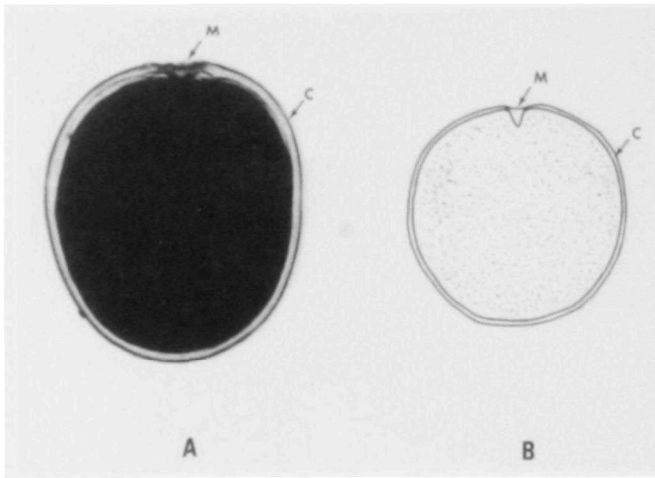

Stage 1: Unfertilized ovum. **Plate 1**

The mature unfertilized ovum is spherical and surrounded by a closely appressed chorion (C). The distinctive micropyle (M) is funnel-shaped with 7 ridges, and protrudes into the yolk mass which consists of yolk platelets mixed with cytoplasm. Cortical granules in the cortical cytoplasmic layer are difficult to observe, but lie on the surface of the whitish, translucent yolk mass. The perivitelline space has not yet formed as seen in Figure A (80x, LS). The opaque yolk mass and cytoplasm of the ovum is represented by small dots in Figure B (80x, LD).

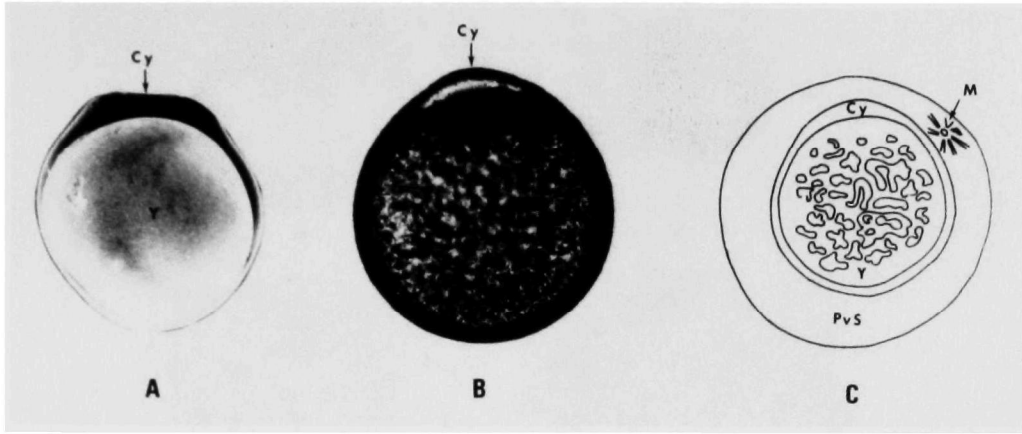

Stage 2: Recently fertilized ovum. **Plate 2**

Following fertilization, the cortical granules break down, starting in the region just under the micropyle. This results in the separation of the chorion from the cytoplasmic layer, with the subsequent formation of the perivitelline space. Large yolk platelets appear to flow together, and the yolk mass becomes clear and remains clear throughout subsequent development. In living embryos, cytoplasm appears to migrate through and around the yolk mass to the animal pole where a low, broad cytoplasmic cap, the blastodisk is forming, establishing the polarity of the embryo.

The chorion has not yet water-hardened and is still soft and fragile, making it difficult to collect embryos without damaging them. The thin plasma membrane which completely surrounds the embryo is covered with microvilli. In later stages, these microvilli will only be found on the blastomeres, but not on the plasma membrane surrounding the yolk mass. Figure A shows the early cytoplasmic cap (Cy) visible above the yolk mass (Y) (80x, SEM). Figure B is a dechorionated live embryo which shows the cytoplasmic cap as an elevated clear region of the peripheral cytoplasm. The yolk has started to clear, although aggregates of large yolk platelets are still present. Note this embryo and all subsequent micrographs of live embryos have been dechorionated (80x, LS). In addition to the cytoplasmic cap and yolk mass, Figure C shows the surrounding chorion (C) with its micropyle (M) and the perivitelline space (PvS) that has formed (80x, LD).

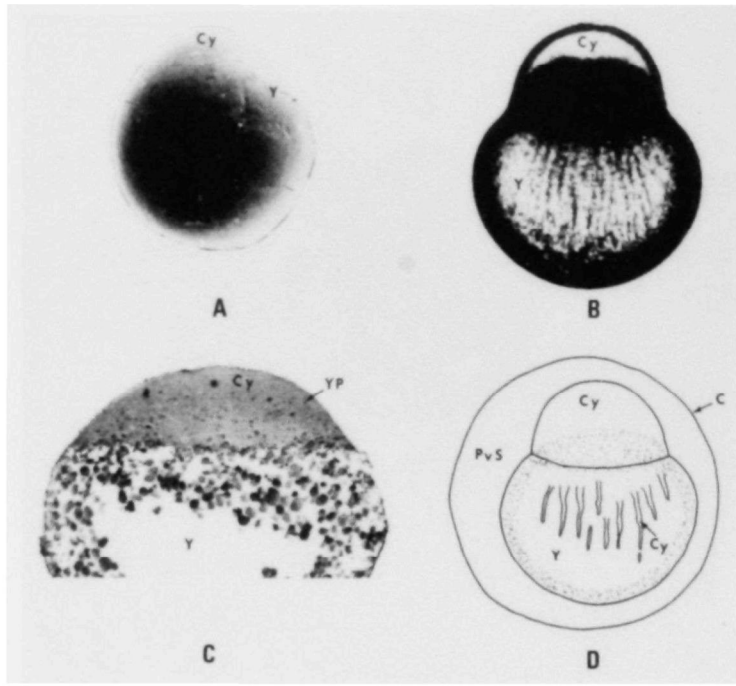

Stage 3: One-celled blastodisc. **Plate 3**

The one-celled blastodisc consists of a large cytoplasmic cap (Cy) which bulges above the yolk mass (Y). Small yolk particles (YP) are found in the granular cytoplasm of the blastodisc. The blastodisc is in close contact with the yolk and is continuous with a thin cytoplasmic layer covering the yolk. In Figure A the cytoplasmic cap is visible as an elevated cap on the yolk mass. The smooth transition of the cytoplasmic cap into the yolk mass seen in this figure is not present in living embryos and is thought to be a fixation artifact (80x, SEM). In Figure B the cytoplasmic cap appears as a clear elevated mass of cytoplasm on the yolk mass (80x, SEM). Figure C shows small yolk particles (YP) visible in the cytoplasm of the cytoplasmic cap (100x, PS). Figure D shows the chorion (C), perivitelline space (PvS), cytoplasmic cap, as well as the residual cytoplasm (Cy) still present in the yolk mass. The solid line shown in this and subsequent drawings represents the ventral border of the early blastomeres. This border is in fact a transition zone rather than an abrupt line (80x, LD).

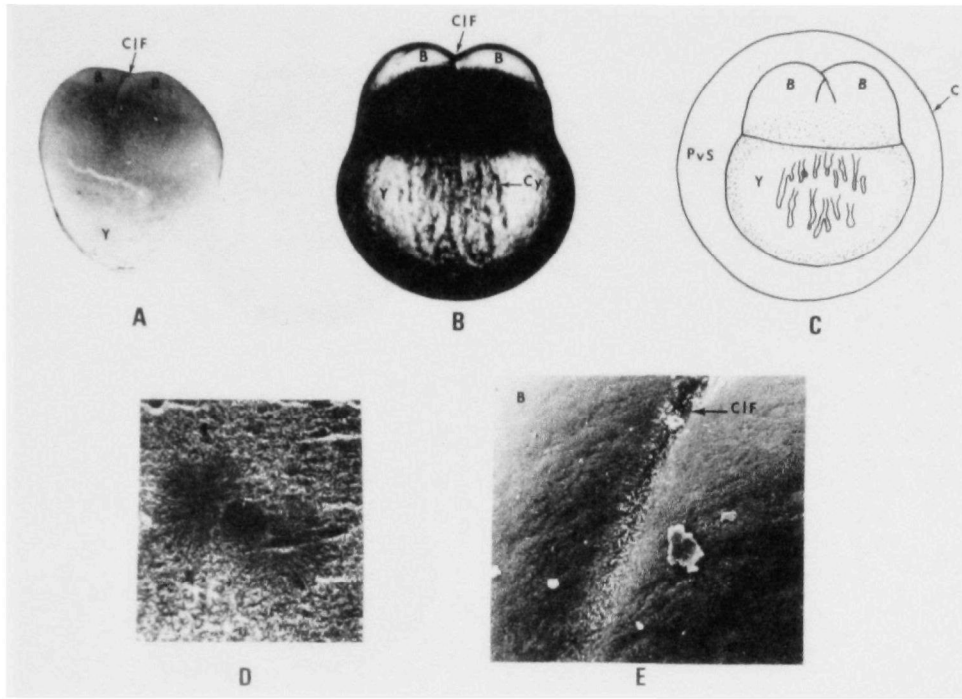

Stage 4: Two-celled blastodisc. **Plate 4**

The first cleavage plane appears initially as a slight depression in the blastodisc and then deepens into a vertical furrow. The first cleavage takes about 7 minutes from start to finish at 25°C. The division is meroblastic and meridional or vertical, resulting in two equal-sized blastomeres (B) which are elevated above the yolk mass (Y). The cleavage furrow (ClF) separating the two blastomeres is visible in Figure A (66x, SEM), Figure B (80x, LS) and Figure C (80x, LD); chorion (C), perivitelline space (PvS). Figure D is a light micrograph that illustrates a metaphase mitotic figure found in the blastomeres prior to the 4-cell stage (200x, PS). Figure E is a higher magnification view of the cleavage furrow separating the two blastomeres (480x, SEM).

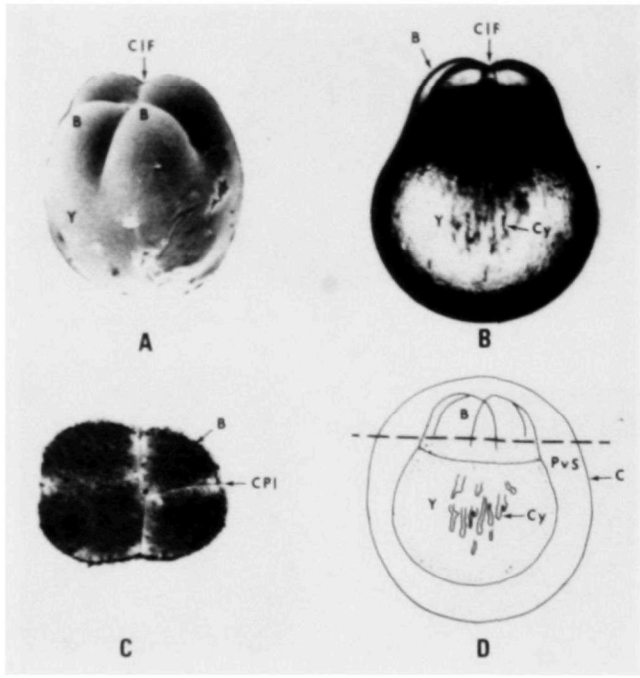

Stage 5: Four-celled blastodisc. **Plate 5**

A second meridional cleavage cuts across the plane of the first at right angles and creates four equal-sized globular blastomeres (B) with their lower surface formed by the yolk (Y) below. This cleavage also takes about 7 minutes at 25°C. Some cytoplasm (Cy) in the yolk is still visible. The embryo rotates freely within the chorion. Figure A shows the four globular blastomeres and the cleavage furrow (ClF) separating them (80x, SEM). The four blastomeres are visible on the yolk mass in Figure B (80x, LS). Figure C is from a serial section and illustrates the cleavage planes that separate the four blastomeres (90x, PS). The dashed line in Figure D indicates the plane of section for Figure C (80x, LD); chorion (C), perivitelline space (PvS).

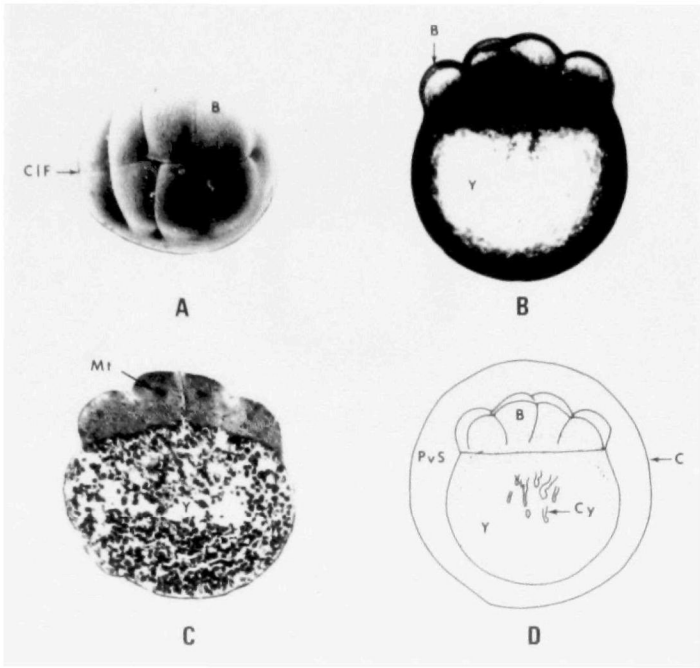

Stage 6: Eight-celled blastodisc. **Plate 6**

Four synchronous meridional cleavages occur parallel to the first cleavage plane, resulting in 8 equal-sized blastomeres (B) arranged in 2 rows of 4 cells each. Minor irregularities in this arrangement are not uncommon. Small yolk granules are visible in the blastodisc cytoplasm adjoining the yolk mass (Y) and extending upward along the cleavage planes. Immediately underlying the blastodisc, yolk particles appear smaller. Cleavage planes cut completely through the blastodisc to the surface of the yolk. Figure A is a dorsal view showing the two parallel rows of four blastomeres (80x, SEM). Figure B offers a side view of four of the eight blastomeres on the yolk mass (80x, LS). Figure C is a serial section showing four blastomeres on the yolk mass. Two of the blastomeres contain distinctive mitotic figures (Mt) (80x, PS). Figure D shows the large perivitelline space (PvS) which is present under the chorion (C) and a limited amount of cytoplasm (Cy) in the yolk (80x, LD).

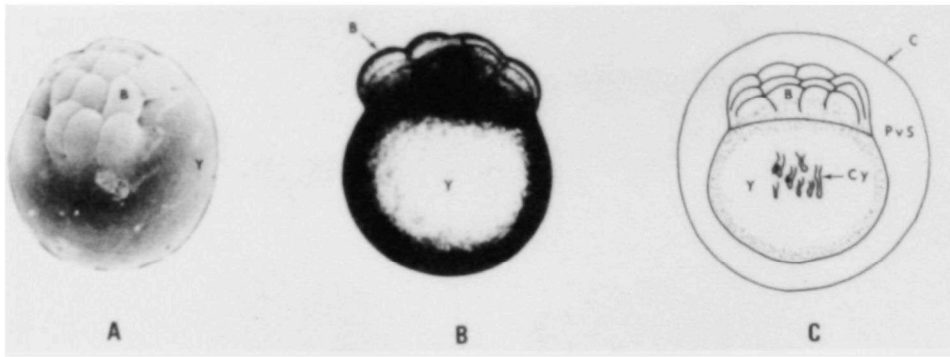

Stage 7: Sixteen-celled blastodisc. **Plate 7**

Cleavage planes are parallel to the second cleavage and at right angles to the first and third. Cleavage is synchronous and generally results in 4 parallel rows of 4 blastomeres (B) of approximately equal size. Cleavage furrows at this stage do not cut completely through the cytoplasm, but leave a continuous layer of cytoplasm adjoining the yolk (Y). This layer of syncytial cytoplasm is the presumptive periblast layer. Figure A shows the blastomeres organized in 4 rows, each consisting of 4 blastomeres (80x, SEM). Figure B is a micrograph of a dechorionated live embryo (80x, LS). Figure C shows the chorion (C), perivitelline space (PvS), blastomeres, as well as the residual cytoplasm (Cy) in the yolk (80x, LD)

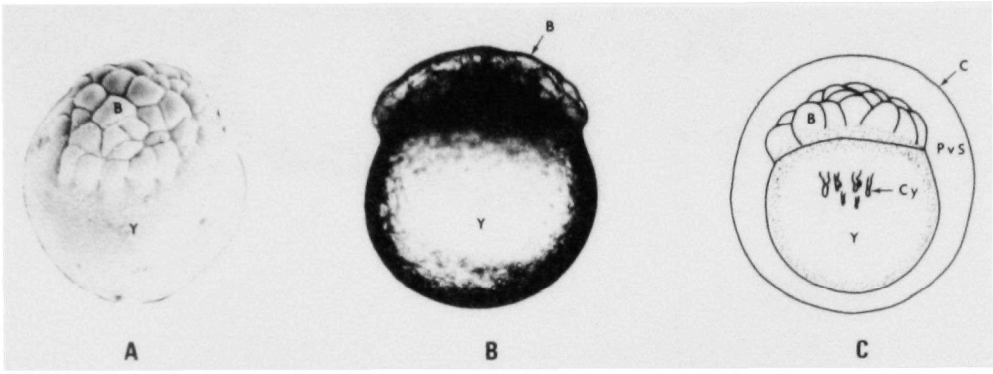

Stage 8: Thirty-two-celled blastodisc. **Plate 8**

Cleavages at this stage start to become asynchronous and difficult to follow. The cleavage planes are no longer strictly perpendicular to yolk mass. Blastomeres (B) are 2 cells deep in the center of the blastodisc. No intercellular spaces are present between blastomeres. The periblast layer of syncytial cytoplasm has migrated from under the blastodisc to form a limited periblast corona. The chorion (C) is now water-hardened and averages 1.4 mm in diameter. Figure A shows approximately 32 blastomeres that form a mound on the yolk mass (Y) (80x, SEM). Figure B is a micrograph of a live dechorionated embryo (80x, LS). Figure C shows the last remnant of cytoplasm (Cy) visible on the yolk mass (80x, LD); perivitelline space (PvS).

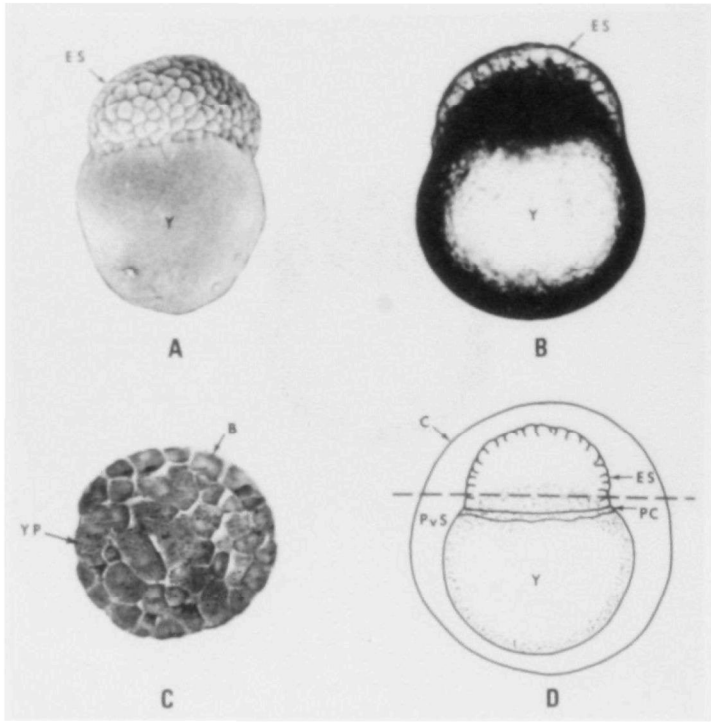

Stage 9: Late cleavage. **Plate 9**

The individual blastomeres form an elevated cap upon the yolk mass. Spaces between the blastomeres are now present. These spaces later become continuous and form the small ventral segmentation cavity or blastocoele. The closely packed outermost layer or envelope of blastomeres form the early epidermal stratum (ES) which surrounds the loosely packed inner cells. The periblast corona (PC) has enlarged. Large yolk particles are visible in the cytoplasm of the deep-lying blastomeres. Figure A shows the early epidermal stratum, the surface layer of blastomeres (80x, SEM). In Figure B note the lack of cytoplasm visible in the yolk (Y) (80x, LS). Figure C is a serial section that shows the individual blastomeres and small yolk particles (YP) within their cytoplasm (80x, PS). Figure D illustrates the limited periblast corona extending from the blastomeres and the surface cells of the epidermal stratum. Plane of section for Figure 9C is indicated by dashed line (80x, LD); chorion (C), perivitelline space (PvS).

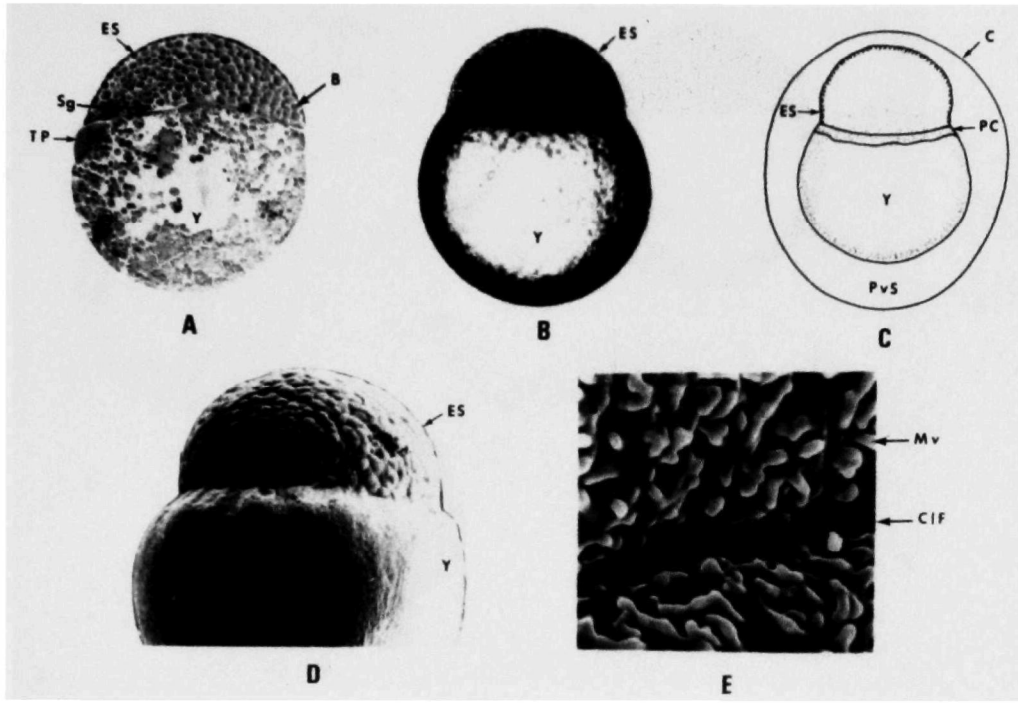

Stage 10: High blastula. **Plate 10**

The epidermal stratum (ES) is distinct and surrounds loosely packed globular interior cells. The blastomere nuclei are large and distinct. The blastoderm rests on the periblast. The periblast corona (PC) has expanded and covers approximately one-fifth of the yolk mass (Y). Periblast nuclei appear to arise at the edge of the blastoderm from divisions of the marginal cells, although mitosis in isolated periblast nuclei is also visible. Large yolk particles appear to be excluded from the blastoderm by the periblast layer. Spaces between blastomeres have increased to form the low broad segmentation cavity (Sg), which is bordered dorsally by globular cells of blastoderm and ventrally by the periblast layer. One portion of the periblast corona has become thickened (TP) and lies immediately adjacent to a thickened region of the blastoderm, where the embryonic shield will form. Microvilli remain present on the plasma membrane of the blastomeres.

Figure A is a serial section that shows the epidermal stratum, consisting of blastomeres (B) which are more squamous in appearance than the deeper-lying blastomeres. The segmentation cavity and the region of thickened periblast are also easily seen (80x, PS). The early periblast corona is seen in Figure B (80x, LS). The periblast corona is more clearly shown in Figure C. The periblast corona has enlarged, while the blastomeres have decreased in size from the previous stage (80x, LD). Figure D shows the epidermal stratum and the underlying yolk mass (120x, SEM). Figure E is a higher magnification micrograph of the blastomeres of the epidermal stratum which are covered with numerous microvilli (Mv). A cleavage furrow (ClF) between two blastomeres is also visible in this figure (7400x, SEM); chorion (C), perivitelline space (PvS).

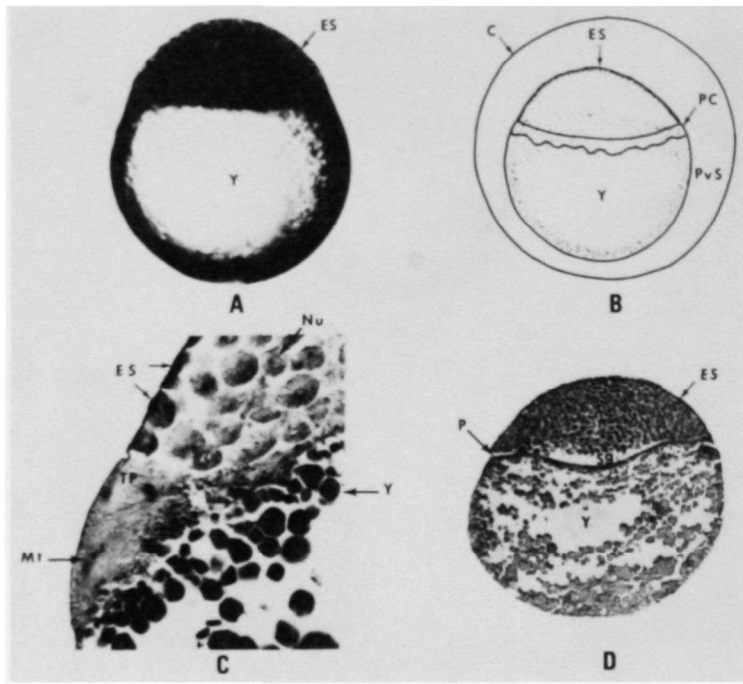

Stage 11: Flat blastula. **Plate 11**

The blastoderm forms a flattened lens-shaped structure called the flat blastula, which caps the yolk mass (Y). There is a further reduction in size, and an increase in number of individual blastomeres. Extensive mitotic activity is visible within the blastomeres and in the periblast nuclei. Cells of the epidermal stratum (ES) are becoming squamous. It is often difficult to distinguish the flat blastula from the early gastrula states in living embryos. The broad segmentation cavity (Sg) or blastocoele is still present.

Figure A shows the small size of the individual blastomeres. Under poor lighting conditions it may be possible to mistake embryos of the high or flat blastula stages for one-celled embryos (80, LS). Figure B is a line drawing that illustrates the further increase in size of the periblast corona (PC) and decrease in size of the blastomeres (66x, LD). Figure C is a serial section that shows mitotic figures in the region of thickened periblast (TP). Also note the epidermal stratum and the distinct nucleus (Nu) of an inner blastomere (200x, PS). Figure D is a serial section that shows the location of the segmentation cavity and the thin layer of underlying periblast (P) (80x, PS); chorion (C), perivitelline space (PvS).

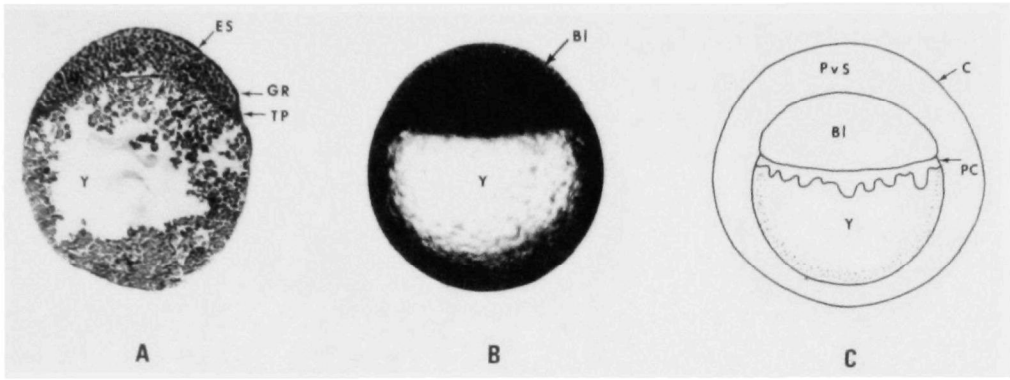

Stage 12: Early gastrula. **Plate 12**

At the onset of gastrulation, the edge of the blastoderm (Bl) becomes elevated to form the early germ ring (GR), which results in a slight depression in the yolk mass (Y). The embryonic shield anlage is faintly visible as an enlargement of one portion of the germ ring that is preceded by a region of thickened periblast. Much mitotic activity is visible in this thickened periblast layer. The number of cells within the central blastoderm has decreased and the segmentation cavity has enlarged.

Figure A shows the slightly thickened profile of the germ ring which forms the advancing edge of the blastoderm (80x, PS). Note much yolk has been lost during sectioning. Figure B shows the flattened mass of cells of the blastoderm that have started to migrate over the yolk mass (80x, LS). Figure C shows the periblast corona (PC) which continues to enlarge and migrate down over the yolk mass (80x, LD); epidermal stratum (ES), thickened periblast (TP), chorion (C), perivitelline space (PvS).

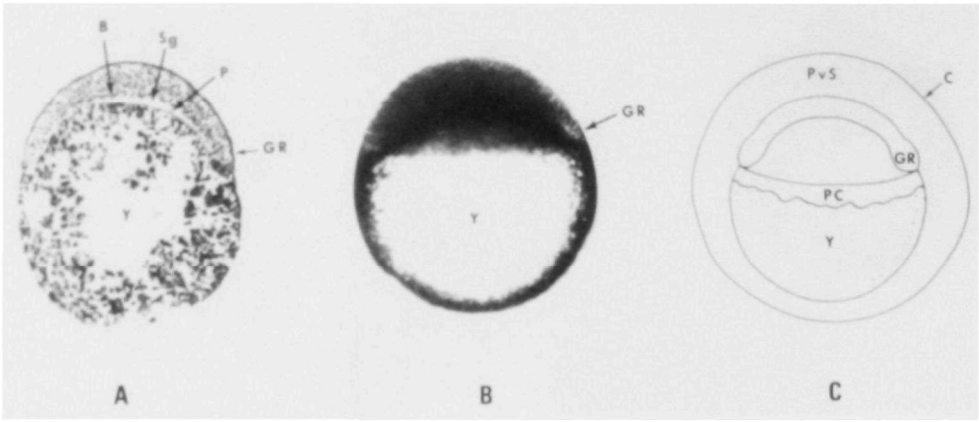

Stage 13: One-quarter epiboly. **Plate 13**

The germ ring (GR) has migrated one-quarter of the way over the yolk mass (Y) and has thickened to become elevated above the blastodisc. Much mitotic activity is evident in the blastomeres (B). An extensive segmentation cavity (Sg) is still present. The periblast corona (PC) is clearly visible in living embryos. Figure A shows the segmentation cavity which is bordered ventrally by the periblast layer and dorsally by the blastomeres. Considerable yolk has been lost during the preparation of this section (80x, PS). Figure B shows the germ ring visible as the edge of the migrating blastoderm (80x, LS). Figure C shows the thickened germ ring, the chorion (C), periblast corona, yolk mass (Y), and perivitelline space (PvS) (80x, LD).

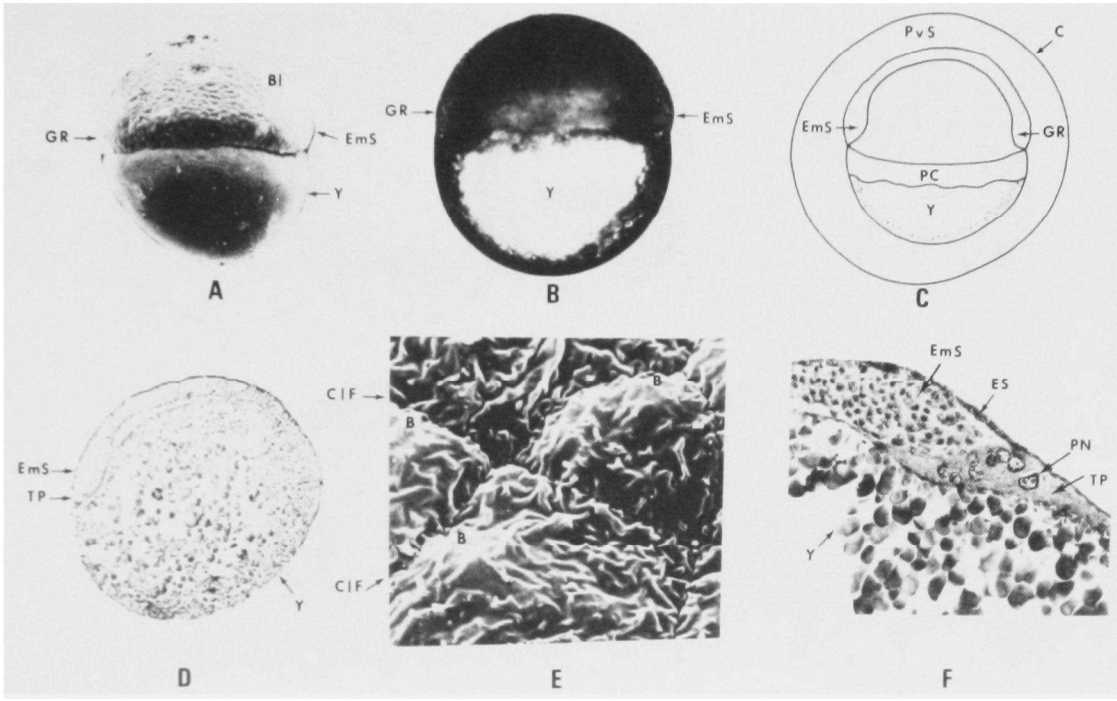

Stage 14: One-half epiboly. **Plate 14**

Epiboly continues with the germ ring (GR) covering one-half of the yolk mass (Y). The inner layer of cells in the germ ring is termed the hypoblast, which is formed by the outward movement of inner cells of the blastoderm (Bl) (Ballard, 1966). The central area of the blastoderm continues to thin. Mitotic figures are no longer visible in the periblast layer, but are evident in the blastomeres. The large oval periblast nuclei are visible in the thickened periblast (TP) layer preceding the embryonic shield (EmS). The embryonic shield appears as a thickened region of the germ ring, slightly closer to the animal pole than is the surrounding germ ring.

Figures A (80x, SEM) and B (80x, LS) show the germ ring and the localized elevated region of blastomeres that make up the embryonic shield . Figure C illustrates the germ ring, embryonic shield, periblast corona (PC), chorion (C), and perivitelline space (PvS) (80x, LD). Figure D shows the embryonic shield and associated region of thickened periblast (80x, PS). Figure E shows the wrinkled appearance of the surface blastomeres. Note the lack of microvilli (3000x, SEM). Figure F is from a serial section that shows the region of thickened periblast with its periblast nuclei (PN) preceding the embryonic shield (200x, PS).

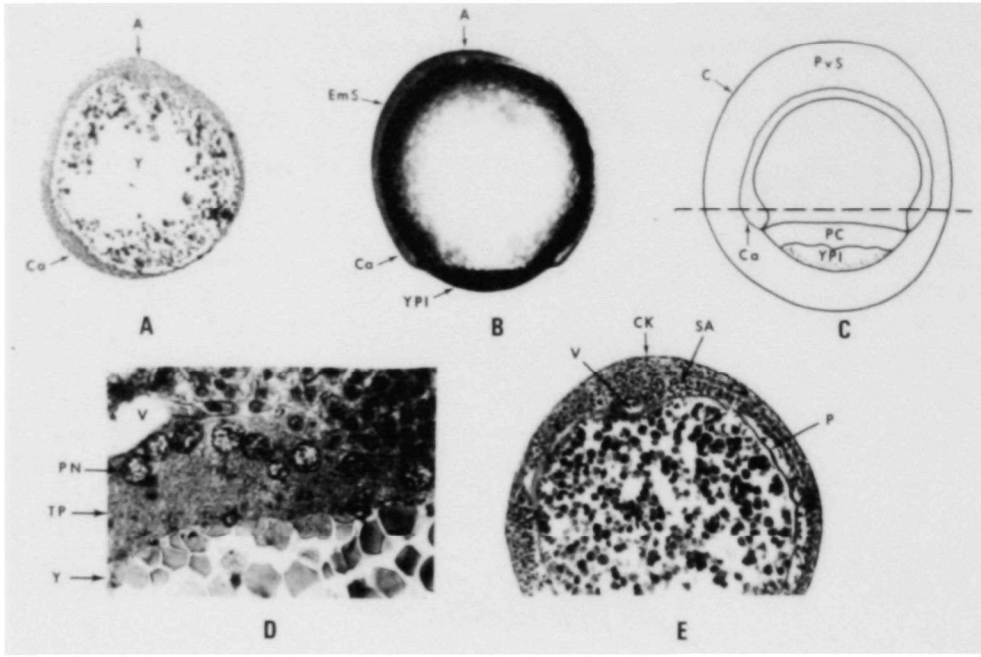

Stage 15: Three-quarters epiboly. **Plate 15**

The germ ring now covers three-quarters of the yolk mass. An unlined vesicle (V) in the periblast (P) under the advancing edge of the embryonic shield is visible in serial sections and creates a depression in the yolk mass. A streak of neuroectoderm cells is behind the embryonic shield. Prior to stage 16, this streak of cells thickens and forms the neural keel anlage. The neural keel, as in other teleosts, forms as a solid mass of neuroectoderm, with the neurocoele forming later in development. The yolk plug (YPl) protrudes slightly from the edge of the advancing germ ring. Mesodermal cells of the somite anlagen (SA) have aligned themselves lateral to the neural keel. Many periblast nuclei (PN) are visible in the periblast layer under the presumptive caudal knob (CK).

Figure A is a sagittal section that shows where the anterior (A) and caudal (Ca) regions of the embryo will form (80x, PS). Figure B shows the thickened ridge of cells that make up the embryonic shield (ES). At this stage the yolk plug has not been covered by the advancing germ ring (80x, LS). Figure C illustrates the future caudal end of the embryo. The plane of section of Figure E is indicated by a dashed line. The periblast corona (PC) almost completely covers the yolk plug (80x, LD). Figure D is a serial section that shows an unlined vesicle (V) and the underlying periblast nuclei in the thickened periblast (TP) (400x, PS). Note the appearance of the yolk mass (Y). Figure E is a serial section that shows the area of the presumptive caudal knob, as well as the lateral somite anlagen. The unlined vesicle and surrounding thickened periblast and periblast nuclei are also visible (100x, PS).

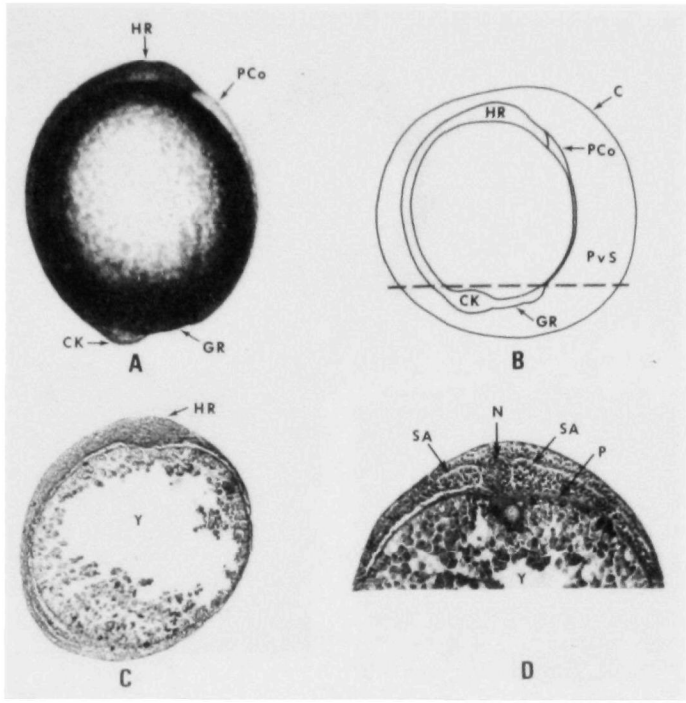

Stage 16: Closure of the germ ring. **Plate 16**

This stage marks the end of epiboly with the closure of the germ ring (GR) over the yolk plug. This process is not synonymous with the closure of the blastopore in amphibians. An elevated cluster of cells is present at the caudal end (Ca) of the embryonic axis where the germ ring closed. A depression in the yolk mass (Y) is visible immediately below this caudal knob (CK). The periblast nuclei continue to proliferate in the periblast layer (P) under the caudal knob. The optic anlagen are visible as two lateral enlargements of head region (HR) which appears as a cluster of cells at the anterior end of the embryo. Anterior and caudal cell clusters are connected by a low broad ridge of cells, the presumptive neural keel. A group of undifferentiated mesodermal cells that form the presumptive notochord (N) are present ventral to this neural keel anlage. There is a migration of lateral mesodermal cells toward the embryonic axis. These cells constitute the somite anlagen (SA).

A thin layer of cells made up externally of the epidermal ectoderm layer which has differentiated from the epidermal stratum and an undifferentiated layer of mesodermal cells internally have lifted free of the yolk mass anterior to the head region to form the precursor to the pericardial coelom. Figure A shows the elevated caudal knob and the head region of the embryo. Note the large fluid-filled presumptive pericardial coelom (PCo) (80x, LS). In Figure B the plane of section for Figure D is indicated by a dashed line. Note the site of closure of the germ ring (66x, LD). Figure C is a serial section that shows the elevated undifferentiated mass of neuroectoderm in the head region (80x, PS). Figure D is a transverse serial section that shows the undifferentiated mesodermal cells of the lateral somite anlagen that flank the notochord (100x, PS); chorion (C), perivitelline space (PvS).

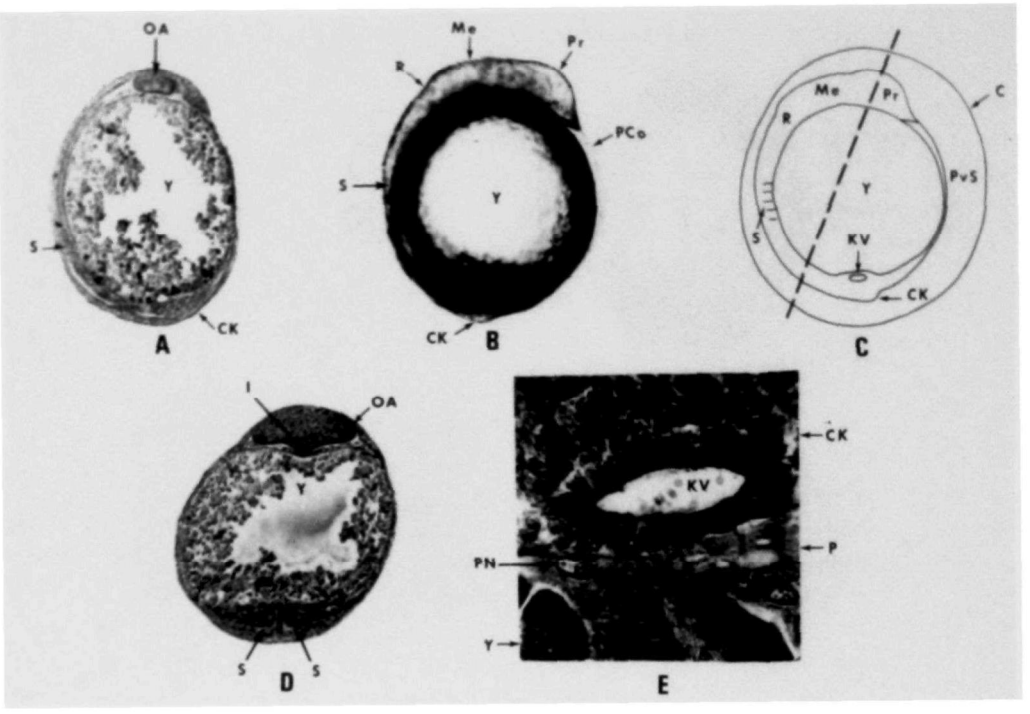

Stage 17: Neurula. **Plate 17**

The prosencephalon (Pr), mesencephalon (Me), and rhombencephalon (R) regions of the brain can be distinguished at this stage. The neural keel consists of a solid wide band of cells that extend caudally from the rhombencephalon. The notochord is visible as a solid rod of mesodermal cells ventral to the neural keel and extends from the rhombencephalon to the undifferentiated caudal knob (CK). The notochord is flanked laterally by mesodermal cells which have differentiated into 4-5 pairs of somites. Kupffer's vesicle (KV) is present as an oval-shaped vesicle ventral to the caudal knob, lined with columnar epithelial cells. Optic anlagen (OA) are visible as lateral swellings of the presumptive diencephalon. The infundibulum anlage starts to form from a ventral evagination of the presumptive diencephalon. Thin sheets of slightly darker-staining neural crest cells are visible both dorsally and ventrally on the lateral aspects of the optic anlagen.

Figure A is a sagittal section that illustrates the optic anlage and the somites (80x, PS) Again note the loss of yolk material from the yolk mass (Y) during sectioning. Figure B shows the three regions of the brain: the prosencephalon, mesencephalon, and rhombencephalon. Also note the anterior-most presumptive pericardial coelom (PCo) (80x, LS). Figure C is a line drawing that shows the three brain regions, prosencephalon, mesencephalon, rhombencephalon, the caudal knob, Kupffer's vesicle, chorion (C), perivitelline space (PvS) and four somites. The plane of section for Figure D is indicated by a dashed line (80x, LD). Figure D is a transverse serial section that shows the optic anlage as lateral evaginations of the prosencephalon. The presumptive infundibulum is present as a ventral evagination of the early diencephalon. Also note the paired block-like caudal somite anlage (80x, PS). In Figure E Kupffer's vesicle bounded by columnar epithelial cells is visible above the thick region of caudal periblast (P). Note the large periblast nuclei (PN) in the caudal periblast (400x, PS).

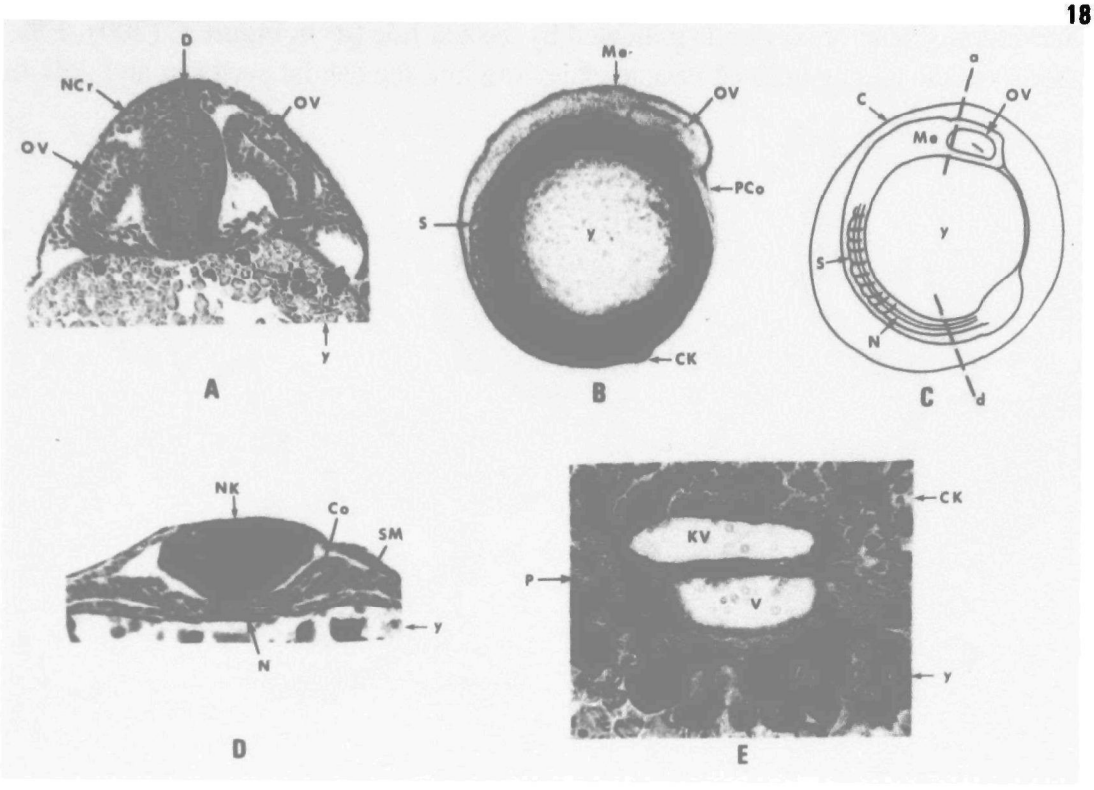

Stage 18: Optic vesicles. **Plate 18**

The site of invagination of the optic vesicles in live embryos appears as a horizontal slit on their lateral aspects. The prosencephalon and optic vesicles are arrowhead-shaped when viewed from above. A depression is forming on the dorsal aspect of the brain between the mesencephalon (Me) and the rhombencephalon. Rudiments of the first and second ventricles of the forebrain are visible as small lateral slits in the anterior end of the prosencephalon. The third ventricular rudiment is a narrow dorsal-ventral slit which is continuous with narrow cavities in the optic vesicles (OV). Cells of the solid neural keel (NK) have become aligned parallel to the yolk mass and have segregated into two lateral masses, although no neurocoele is present. The neural keel is oval in cross-section anteriorly and becomes triangular caudally. A large infundibulum extends ventrally from the diencephalon (D). Cells of the notochord (N) are elongating and becoming vacuolated.

Caudally, the notochordal cells become increasingly disorganized until they grade into undifferentiated mesoderm of the caudal knob (CK). Several unlined vesicles (V) are present in the thick periblast layer (P) ventral to Kupffer's vesicle (KV). The number of periblast nuclei in the caudal periblast continues to increase. The pericardial coelom (PCo) is present as a fluid-filled sac anterior to and ventral to the first one-third optic vesicles. Nine to ten pairs of somites (S) are present. Somites are 6-7 cells thick adjacent to the notochord, but taper off into lateral plate mesoderm laterally and into flattened segmental mesoderm (SM) caudally. A small coelomic cavity (Co) is present in the segmental mesoderm. There is no indication of circulatory or digestive system rudiments. Neural crest cells (NCr) are visible as diffuse masses of cells dorsal-lateral and ventral-lateral to the diencephalon and mesencephalon, and as diffuse masses of cells lateral to the nerve cord in mid and caudal regions. Figure A is a transverse section that shows the optic vesicles situated lateral to the diencephalon. Note the lack of neurocoele in the diencephalon. Neural crest cells are visible dorsal and lateral to the diencephalon. Plane of section is represented by the dashed line (a) in Figure C (200x, PC). Figure B illustrates the optic vesicles, pericardial

coelom, caudal knob, somites and translucent yolk mass (Y) in a live embryo (80x, LS). Figure C is a line drawing that illustrates the optic vesicles, caudal knob, notochord, and somites (80x, LD). In Figure D the triangular neural keel is visible above the notochord. A small coelomic cavity is visible in the segmental mesoderm. Plane of section is indicated by dashed line (d) in Figure C (200x, PS). Figure E shows Kupffer's vesicle and an unlined vesicle extending into the caudal periblast and yolk mass (400x, PS).

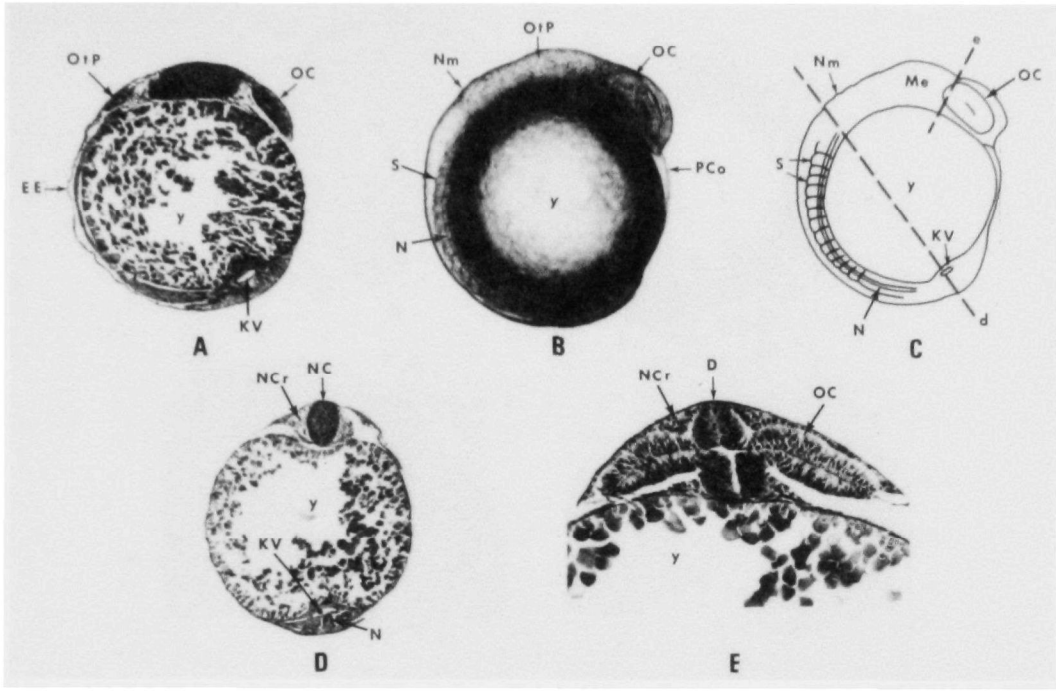

Stage 19: Neuromeres. **Plate 19**

Neuromeres (Nm) are visible as a series of small enlargements or evaginations in the dorsal myelencephalon. A neurocoele is present only in the form of the reduced brain ventricles. The cavity within the optic cups (OC) has increased in size. The ventrally located pericardial coelom (PCo) has enlarged both anteriorly and posteriorly. The otic placodes (OtP) are visible as a pair of lateral thickenings in the epidermal ectoderm (EE) in the rhombencephalic region. The 14 pairs of somites (S) are bounded by a layer of columnar cells and have condensed to form more block-shaped segments. Notochordal (N) cells are becoming increasingly vacuolated, and the notochord has increased in length anteriorly. A thick periblast layer with its nuclei and Kupffer's vesicle (KV) are present below the somewhat flattened caudal knob. The embryo is bounded by a squamous epithelial layer of ectoderm. Neural crest cells (NCr) continue to migrate around the brain and nerve cord (NC).

In Figure A the otic placodes are visible in this sagittal section as thickenings in the epidermal ectoderm. Note that Kupffer's vesicle and the optic cup are still prominent structures (80x, PS). In Figure B a large optic cup is visible in the prosencephalon. The otic placode is visible as a slightly clear region in the rhombencephalon (80x, LS). In Figure C neuromeres are visible as a series of small evaginations in the dorsal rhombencephalon. Fourteen somites are shown as are the distinctive optic cup and prosencephalon. Planes of section for Figures D and E are indicated by dashed lines (d) and (e), respectively (80x, LD). Figure D is a transverse serial section that shows the solid nerve cord posterior to the rhombencephalon. The notochord and Kupffer's vesicle are also visible in the caudal region (80x, PS). In Figure E the posterior edge of the optic cup is visible, as is its connection with the diencephalon (D). Neural crest cells are visible as dorsal and ventral masses of cells lateral to the diencephalon (150x, PS). Note that this stage and all subsequent stages show figures of dechorionated embryos.

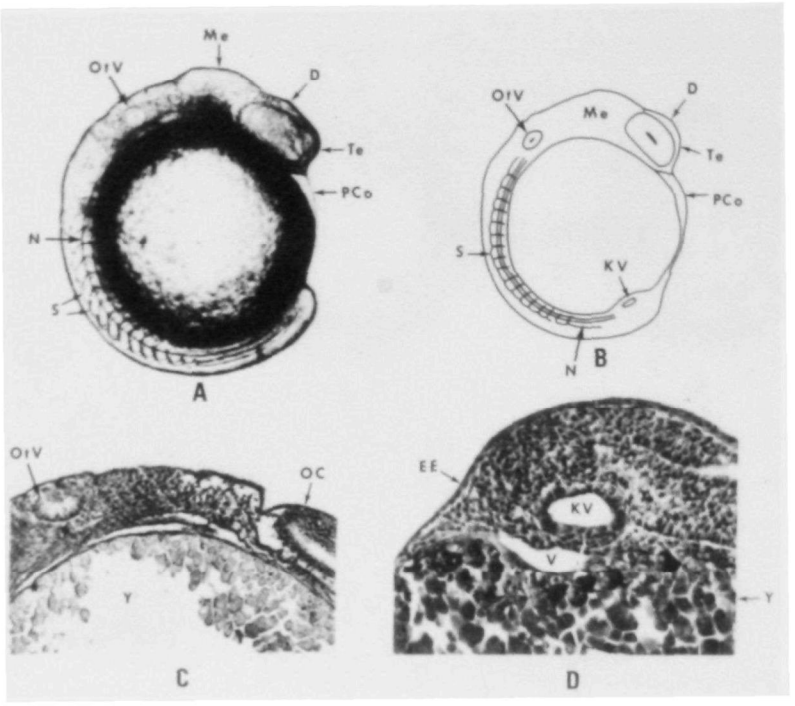

Stage 20: Otic vesicles. **Plate 20**

Otic vesicles (OtV) have formed, and each possesses a small lumen surrounded by columnar cells with peripherally located nuclei. The three primary brain regions and neuromeres are easily distinguished in living embryos. The mesencephalon (Me) is markedly elevated above the rest of the brain. 16 pairs of somites (S) are becoming chevron-shaped. The periblast nuclei are moving anteriorly out of the caudal periblast layer. The pericardial coelom (PCo) continues to migrate posteriorly.

In Figure A the otic vesicle is visible as a clear region lateral to the rhombencephalon. The mesencephalon is elevated above the rest of the brain. Sixteen somites, the notochord (N), the diencephalon (D), telencephalon (Te), and pericardial coelom are also visible (80x, LS). Figure B shows the location of Kupffer's vesicle (KV) as well as the other structures identified in Figure A (80x, LD). In Figure C the small lumen and columnar cells that make up the otic vesicle are visible in sagittal section (200x, PS). In Figure D Kupffer's vesicle and an unlined ventral vesicle (V) are visible in the caudal region. The embryo is bounded by the epidermal ectoderm layer (EE) (400x, PS).

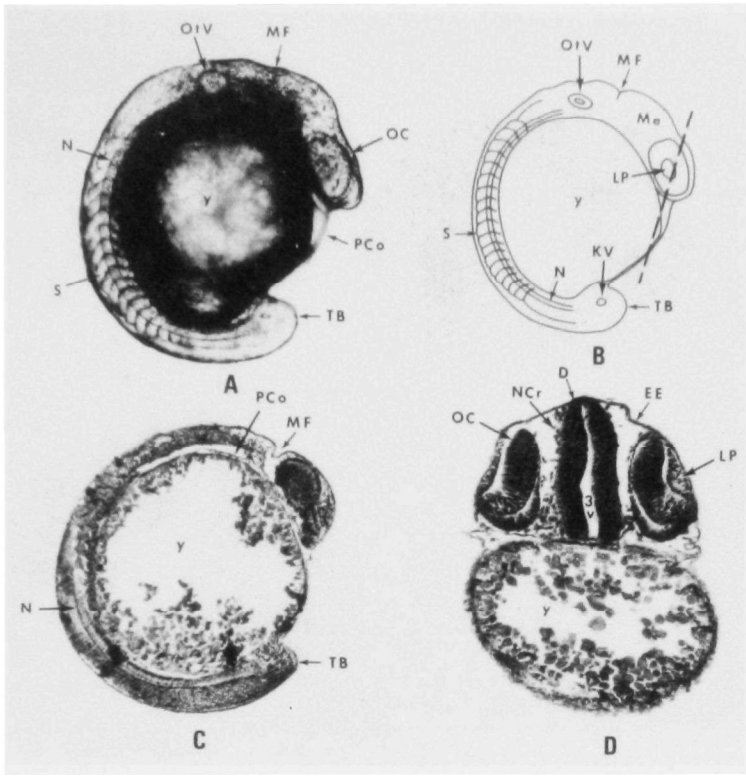

Stage 21: Tailbud. **Plate 21**

The tailbud (TB) has formed and is starting to lift free of the yolk mass (Y). The 18-20 pairs of somites (S) are becoming increasingly chevron-shaped. A fissure (MF) separating the mesencephalon (Me) and the metencephalon has formed perpendicular to the embryonic axis. The aqueduct of Sylvius connects the slightly enlarged third ventricle (3v) with the fourth ventricle (4v). The spinal cord is oval in transverse section and contains a narrow neurocoele. The olfactory placodes (O1P) are visible as a pair of thickenings in the ectoderm between the optic cups (OC). The lens placodes (LP) are present as rounded masses of undifferentiated ectodermal cells, extending into the optic cup but still attached to the epidermal ectoderm (EE). The periblast under the tailbud has become reduced in size. Periblast nuclei continue to migrate anteriorly in the periblast or yolk-sac syncytium. There is no indication of the gut anlage at this stage. A broad ventral mass of mesoderm extending caudally from the optic cups will form the heart anlage in later stages. The pericardial coelom (PCo) continues to migrate posteriorly.

Figure A shows the tailbud, enlarged otic vesicle (OtV), optic cup, and the mesen-metencephalon fissure (MF). Note the increase in somite number since the previous stage (80x, LS). In Figure B the lens placode which is not visible in Figure A is illustrated in this line drawing. The plane of section of Figure D is indicated by the dashed line (80x, LD). Figure C is a sagittal section that shows how far posterior the pericardial coelom is located. Also note the elongated cells of the notochord (80x, PS). Figure D is a transverse section that shows the lens placode still attached to the epidermal ectoderm. Scattered neural crest cells are visible lateral to the diencephalon. Note the enlarged third ventricle and the scattered neural crest cells (NCr) on the lateral aspects of the diencephalon (D) (120x, PS).

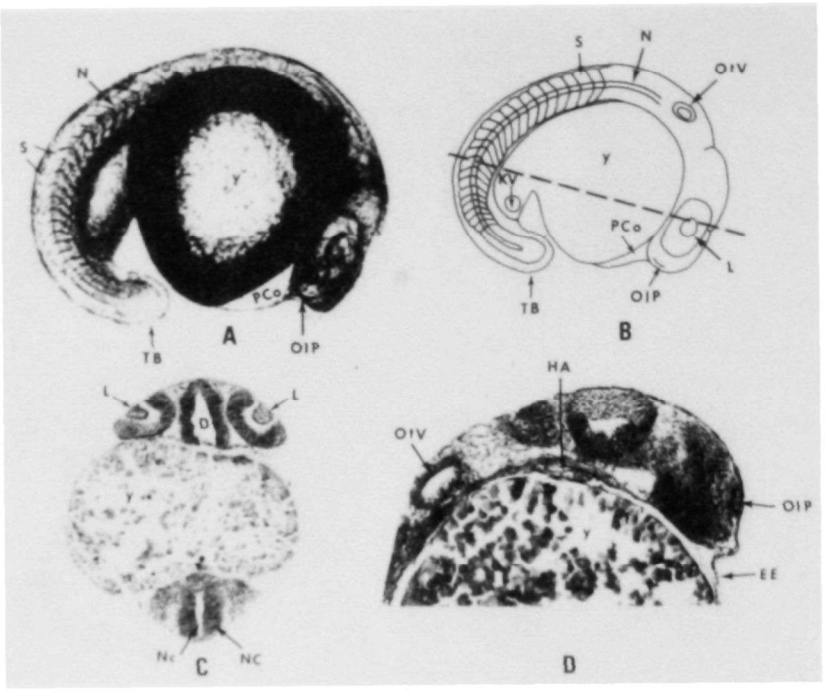

Stage 22: First movements. **Plate 22**

Weak twitching movements are first observed in living embryos. The tailbud (TB) has elongated and is free of the yolk mass (Y). Brain ventricles and the neurocoele (Nc) of the nerve cord (NC) have enlarged. The olfactory placodes (OlP) have sunk into to epidermal ectoderm (EE) to form the olfactory pits which are visible in living embryos. The otic vesicles (OtV) have enlarged. The lens has formed and is clearly visible in the optic cups, which remain connected to the diencephalon (D) by a hollow cord of cells. Muscle fiber cell precursors in the 20 somite (S) pairs are elongating and becoming multinucleated. The pericardial coelom (PCo) has enlarged considerably. The heart anlage (HA) is visible as an anterior-ventral evagination from a broad sheet of mesoderm located under the mesen-metencephalic fissure (mesen-metencephalic fold). The embryonic coelom is visible as a small cavity in the mesoderm lateral to the somites. Neuromast anlagen are visible as columnar thickenings of cells in the epidermal ectoderm lateral to the nerve cord in the midregions of the embryo.

Figure A clearly illustrates the enlarged tailbud and pericardial coelom (80x, LS). Note the appearance of the somites and notochord (N). In Figure B the olfactory placode is indicated by a line in the anterior telencephalon. The lens (L) and otic vesicle (OtV) have enlarged and are easily distinguished in living embryos. The plane of section for Figure C is indicated by a dashed line (80x, LD). In Figure C the enlarged lens is visible in the optic cups. Note the large neurocoele in the nerve cord (80x, PS). Figure D is a sagittal section that shows the enlarged lumen of the otic vesicle. The heart anlage is visible as two sheets of mesoderm, the early endocardium and epimyocardium layers. The olfactory placode is visible as a thickening in the epidermal ectoderm in the anterior telencephalon; yolk (Y) (200x, PS).

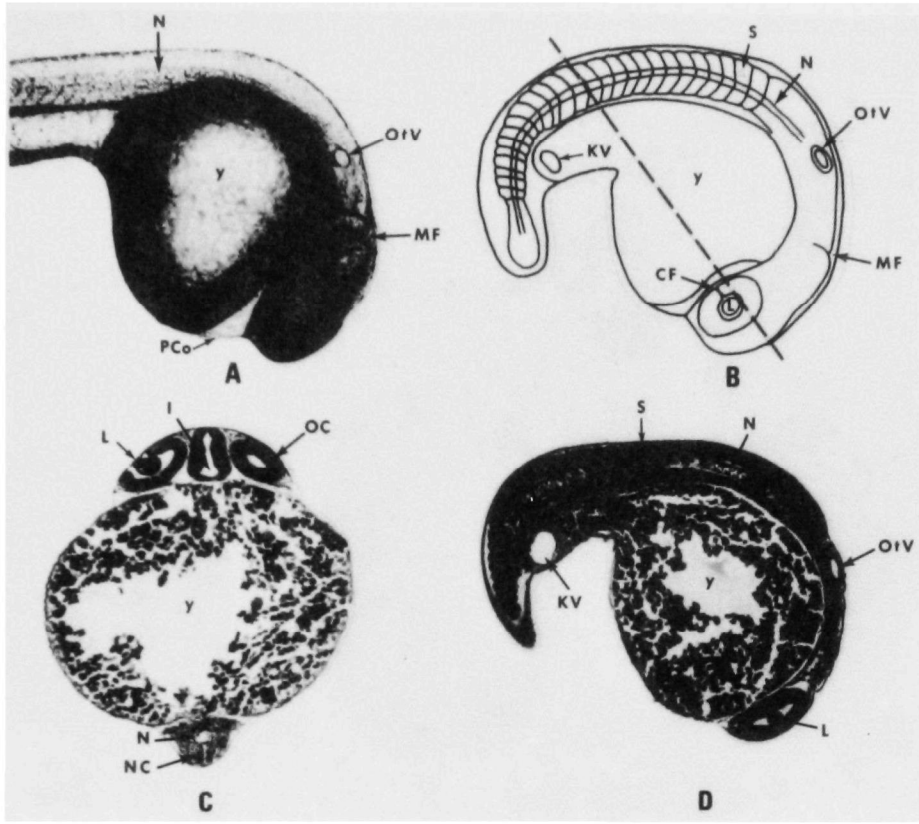

Stage 23: Heartbeat. **Plate 23**

The S-shaped tubular heart lies in a depression in the yolk (Y) ventral to the left eye. A colorless fluid is visible moving in the heart as it beats sporadically, although no peripheral circulation is present. Blood islands are forming as clumps of cells on the yolk mass. The embryo exhibits extensive tail thrashing movements. The brain ventricles have enlarged, and the roof of the rhombencephalon has started to become thinner. The mesen-metencephalon fissure (MF) is more pronounced than previously. The large infundibulum (I) has expanded laterally. The lens (L) and the ventral choroid fissure (CF) are distinct in living embryos. Periblast nuclei continue to migrate laterally and anteriorly from the periblast region under Kupffer's vesicle (KV). In the caudal region, the dorsal and ventral medial fin folds are visible as thickened evaginations in the epidermal ectoderm. Muscle fibers remain immature, but continue to elongate. The olfactory pits are lined with columnar epithelial cells and are located medial to the optic cups (OC). Paired pronephric ducts are present in the caudal region as a pair of thin-walled laterally located tubes, each having a small lumen. They merge anteriorly to form a single thin-walled structure, the urinary bladder anlage.

Figure A shows the large pericardial coelom (PCo) and otic vesicle (OtV). The yolk mass is considerably reduced in size compared to the rest of the embryo (80x, LS). In Figure B the ventral choroid fissure and enlarged somites (S) are visible. The mesen-metencephalic fissure and otic vesicle are easily distinguished in living embryos. The plane of section of Figure C is indicated by the dashed line (80x, LD). In Figure C the large lens is visible in the optic cup. The infundibulum has expanded laterally. The ventral nerve cord (NC) and dorsal notochord (N) are visible in the caudal region (80x, PS). Figure D is a sagittal section that shows the somites. Their distinctive appearance is due to the elongated muscle fibers. The optic cup, lens, and otic vesicle are clearly visible. Note the large Kupffer's vesicle and the vacuolated cells of the notochord (80x, PS).

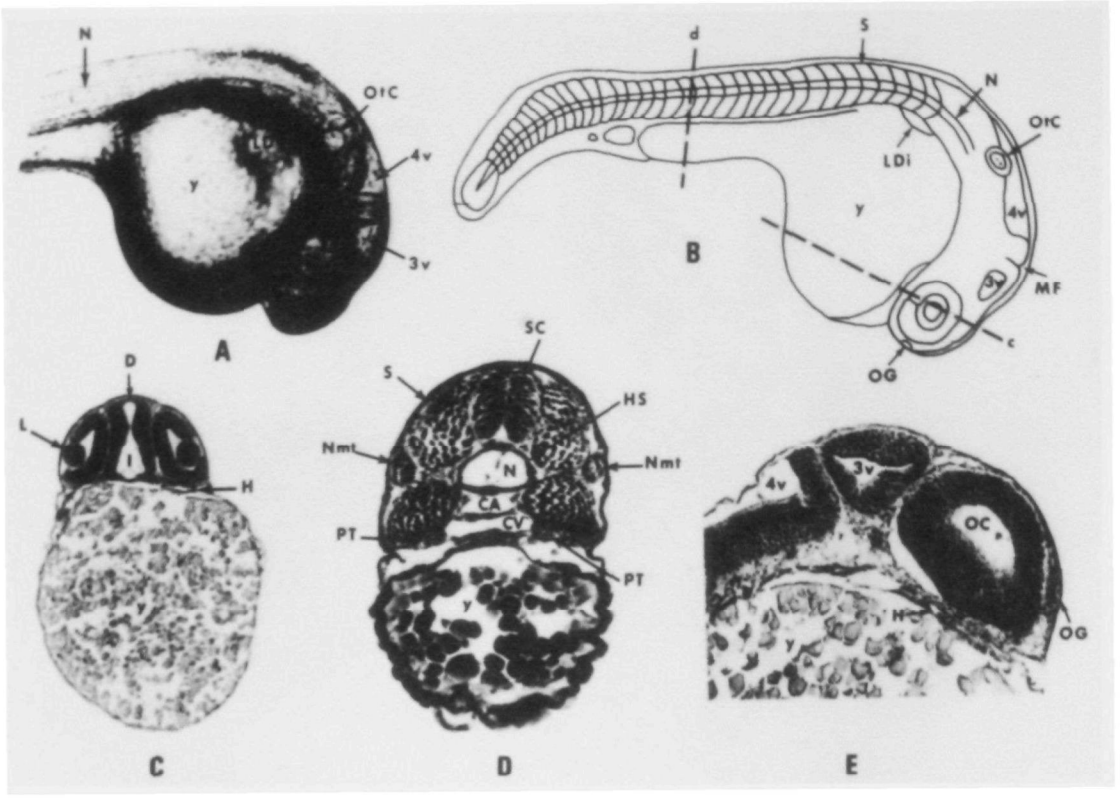

Stage 24: Circulation. **Plate 24**

Blood islands resting on the yolk mass (Y) consist of light yellow aggregations of cells. These cells are being washed into the large common cardinal veins (cc) by the blood flow. Colorless nucleated blood cells leave the heart (H) and enter the ventral aorta which divides anteriorly into the internal carotid and hyaloid arteries, and posteriorly to form the dorsal aorta. The large caudal artery (CA) lies immediately under the notochord (N) and extends to the sixth precloacal somite (S). The caudal vein (CV) is immediately ventral to the caudal artery. Otoliths are visible as two small concretions in each otic capsule (OtC). The lens (L) has enlarged and is surrounded by a single layer of columnar epithelium. The dorsal and ventral median fin folds continue to form anteriorly. The gut can be seen as a thin-walled ventral tube of endoderm extending from the mesencephalon to the proctodeum. The proctodeum is visible as an invagination in the epidermal ectoderm ventral to the terminus of the hindgut. The liver diverticulum (LDi) is present as a mass of tissue budding off from the ventral foregut below the posterior myelencephalon.

The paired pronephric ducts (PT) are ventral and lateral to the caudal vein, and are bounded by a single layer of columnar cells. Neuromasts (Nmt) of the lateral line system are visible as condensations of tissue under the epidermal ectoderm lateral to the somites (S). The tail has elongated and the embryo now possesses 35 to 37 pairs of somites. A lighter-staining region (white matter) consisting of axons is visible on the lateral aspects of the diencephalon (D) medial to the optic cups (OC). The third and fourth ventricles have enlarged. Cells of the notochord (N) are highly vacuolated. The notochord is encased in a thin hyaline sheath (HS).

In Figure A the distinctive third (3v) and fourth (4v) brain ventricles are easily seen in living embryos (80x). In Figure B the otoliths are visible as a pair of small concretions in the otic vesicle. The liver diverticulum appears as a depression in the yolk sac. The olfactory groove (OG) is visible in the anterior telencephalon. Planes of section for Figures C and D are represented by dashed lines (c) and (d), respectively (80x, LD). In Figure C the heart is visible as a thin tube of mesoderm under the optic cup. The

lens is surrounded by columnar epithelium and infundibulum (I) (80x, PS). Figure D is a transverse serial section that shows the spinal cord (SC), the caudal artery and vein and the notochord which is encased in a hyaline sheath. The lens-shaped neuromasts are visible lateral to the caudal artery (200x, PS). Figure E is a sagittal serial section that shows the optic cup, third and fourth ventricles, and heart (200x, PS).

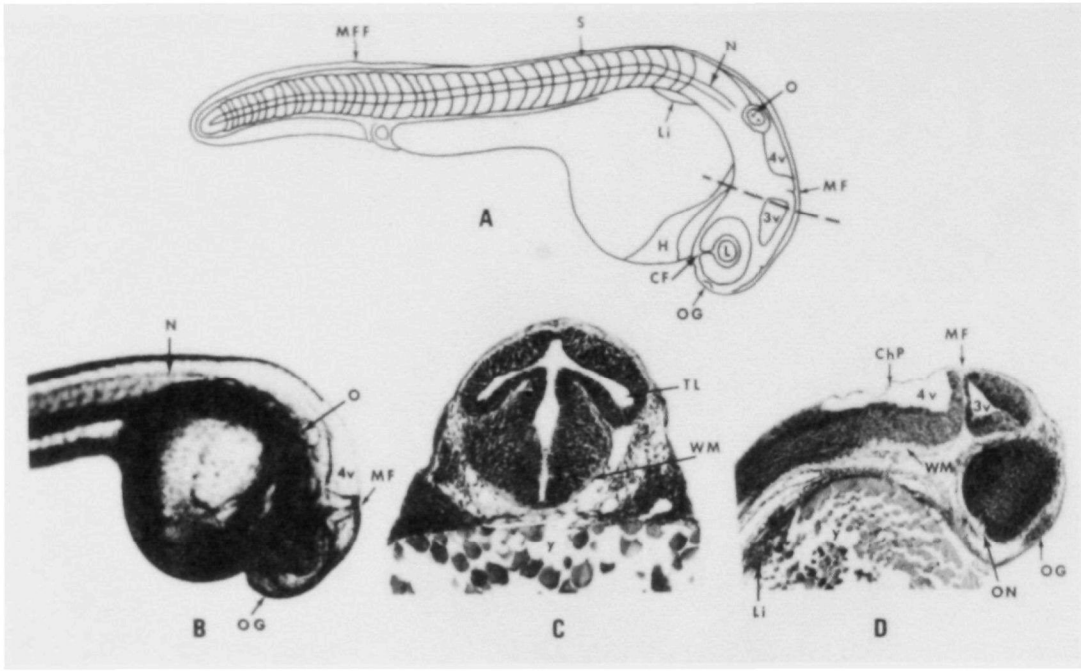

Stage 25: Retinal pigmentation. **Plate 25**

The outermost layer of flattened epithelial cells surrounding the optic cup has become pigmented, giving the optic cups a darkened color. The head is beginning to lift free of the yolk mass. The marked cephalic flexure occurs at the mesen-metencephalic transition. The optic nerve (ON) leaves the optic cup through the ventral choroid fissure (CF). The white matter (WM) continues to increase in volume on the ventral surface of the brain and spinal cord. The tectal lobes (TL) are visible as evaginations on the dorsal and lateral surfaces of the mesencephalon. On the ventral surface of the anterior yolk mass, a large sac of blood is filled by the cardinal veins and drained by the sinus venosus. Blood islands are still present on the yolk sac. The heart (H) has a definite S-shape and lies primarily on the yolk sac under the right optic cup. Blood flow extends to the third postcaudal somite (S). Small thickenings in the epidermal ectoderm (EE) are located throughout the head region and surrounding the cloacal opening. The median fin fold (MFF) continues to form anteriorly.

The lens-shaped neuromasts of the lateral line system are visible at intervals below the epidermal ectoderm lateral to the somites in the caudal region. Masses of mesenchyme and neural crest cells are condensing lateral and ventral to the rhombencephalon near the otic capsule. The anterior pituitary anlage is visible as an undifferentiated mass of ectodermal cells budding off the dorsal pharynx. Pharyngeal pouches 5 and 6 are visible as lateral pockets in the pharyngeal region anterior to the otic capsule. Axons extend from a placode posterior to the optic cups toward the mesencephalon, and will later become part of cranial ganglion V. The thin roof of the rhombencephalon which is the site of formation of the choroid plexus is clearly visible in living embryos. Liver (Li) tissue continues to proliferate. Embryos are quite active, exhibiting frequent thrashing movements.

In Figure A the median fin fold is easily visible in living embryos. The somites, heart, liver, and otoliths (O) continue to differentiate. The choroid fissure is clearly visible in the optic cup. The plane of section for Figure C is indicated by the dashed line (80x, LD). In Figure B the olfactory groove (OG) is

visible in the anterior telencephalon. The otoliths appear as dark concretions in the otic capsule (80x, LS). Figure C is a transverse section that shows the lateral tectal lobes and the thin layer of white matter (200xPS). Figure D is a sagittal serial that shows the posterior choroid plexus which forms the roof of the rhombencephalon. The optic nerve is visible as a lightly stained region ventral to the optic cup. Liver tissue forms a depression in the yolk mass. Note the distinctive olfactory groove (OG) (100x, PS).

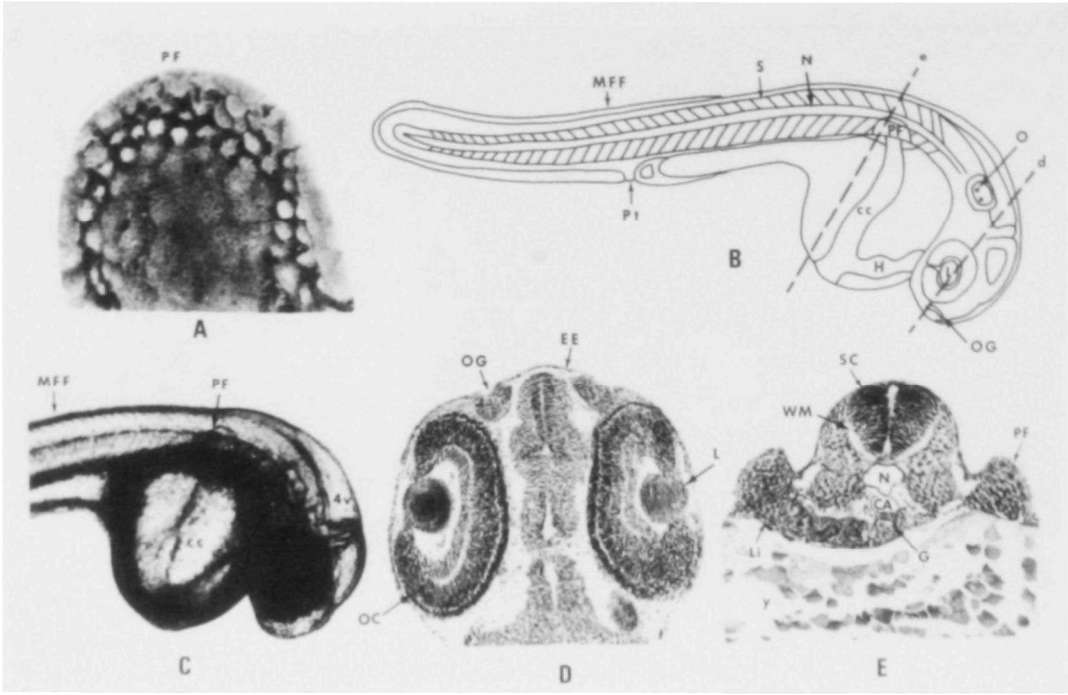

Stage 26: Intersegmental arteries. **Plate 26**

The two pectoral fin (PF) buds which first became visible at about 45 hr have enlarged. Blood flow is seen for the first time in the intersegmental arteries. Blood cells are becoming more pigmented, and blood flow now extends to the fourth postcaudal somite (S). The cardinal veins are well-defined and lie in depressions in the shrinking yolk sac. The hindgut (G) consists of a small lumen surrounded by a single layer of columnar epithelium and is located immediately ventral to the caudal vein. The lumen of the hindgut enlarges just anterior to the cloaca. The sinus venosus, atrium, ventricle, and conus arteriosus of the heart can be distinguished in living embryos. Powerful ventricular contractions cause the head of the embryo to bob up and down. Circulation has increased in the head plexus. The eyes have a silvery color. The embryo continues to elongate as the head lifts free of the yolk sac.

The enlarged olfactory grooves (OG) are lined by a layer of columnar cells. The epiphysis anlage appears as a small evagination from the roof of the diencephalon. White matter (WM) continues to increase in volume on the ventral and lateral surfaces of the brain and spinal cord (SC). Kupffer's vesicle persists anterior to the cloaca. The highly vacuolated cells of the notochord (N) are transparent and stacked in layers. The notochord tapers and terminates ventral to the anterior end of the otic capsule. The otic capsule is no longer oval; instead, it is narrower at its base where the enlarged otoliths (O) are located.

There is no indication of a stomodeum at this stage, but the pharynx has enlarged laterally. The liver continues to enlarge. Muscle fibers continue to elongate and are developing the banding pattern typical of striated muscle. Neuromasts have continued to proliferate and to migrate anteriorly. The eyes are connected to the diencephalon by the optic nerve. A small fold of cells connects the spinal cord with the dorsal fin fold. The pituitary anlage is visible as a compact mass of cells ventral to and closely appressed to the large infundibulum. The squamous epidermal-ectodermal (EE) cells are pentagon-shaped.

Figure A is a SEM micrograph that shows a pectoral fin with its surface covered by epidermal ecto-

derm cells (540x, SEM). Figure B is a line drawing that illustrates those structures easily seen in living embryos and in serial sections: median fin fold (MFF), proctodeum (Pt), heart, common cardinals (CC), otoliths, olfactory groove. The plane of section of Figures D and E are shown as dashed lines (d) and (e), respectively (80x, LD). In Figure C the median fin fold, otoliths, common cardinals, olfactory groove, pectoral fins, fourth ventricle (4v) and optic cup are visible (80x, LS). Figure D is a frontal serial section that shows the lens in the optic cup (OC) as well as the large olfactory grooves in the epidermal ectoderm (200x, PS). Figure E shows white matter on the ventral and lateral surfaces of the spinal cord. Note the pectoral fins, notochord, caudal artery (CA), liver tissue (Li), and gut with a small lumen (200x, PS).

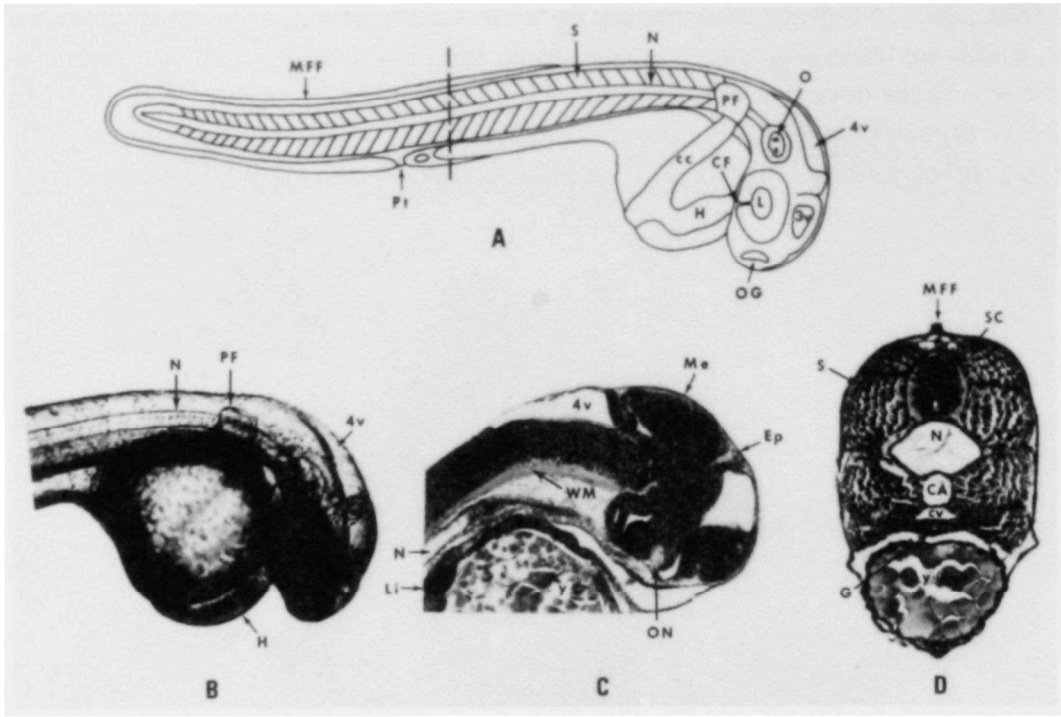

Stage 27: Horizontal duct. **Plate 27**

The walls of the otic or auditory capsule (OtC) have thickened ventrally and thinned dorsally where the horizontal duct is forming. The paired otoliths (O) are oval-shaped and have become perpendicular in orientation to each other. The olfactory grooves have elongated and are closely associated with the anlage of the olfactory lobes, although no connection is visible yet.

A strong blood flow is present in the intersegmental arteries. A short vessel extends caudally beyond the turnaround point of the caudal artery. Radial striations centered around the tip of the notochord (N) have started to form in the caudal fin. The medial fin fold (MFF) continues to enlarge and extend anteriorly. The surface thickenings in the epidermal ectoderm noted in previous stages are darkening. The notochord extends anteriorly to the mesen-metencephalic fissure and lies just dorsal to the pharynx. A small unlined vesicle and scattered large periblast nuclei are present at the posterior end of the yolk sac just anterior to the cloaca (Cl).

The presumptive cone cells have elongated inside the pigmented layer of the eye. The precursors of cranial ganglia IX and X are visible in serial sections as dorsal-lateral placodes sending bundles of axons toward the myelencephalon. White matter continues to increase in volume. The two lateral cavities of the tectal lobes have enlarged in the mesencephalon. Neuromasts of the lateral line system are visible in lateral pairs throughout the head region. The mandibular, hyoid, and pharyngeal arches 3 and 4 are visible. Masses of tissue which later form the parachordal and trabecular cartilages are condensing dorsal to the pharynx. The early elements of the lower jaw are visible in sections as lateral and ventral condensations of tissue of the pharynx.

Figure A is a line drawing that illustrates the perpendicular orientation of the otoliths in the otic capsule. The notochord, pectoral fins (PF), olfactory groove (OG), somites (S), and heart (H) continue to differentiate. Plane of section of Figure D is indicated by the dashed line (80x, LD). In Figure B the large heart is visible on the anterior yolk sac. The notochord, fourth ventricle (4v) and pectoral fins are

easily seen in living embryos (80x, LS). Figure C is a sagittal serial section that shows white matter on the ventral hind brain. The thick optic nerve (ON) and extensive liver (Li) are also visible. The epiphysis is visible as an evagination in the roof of the diencephalon (100x, PS). Figure D is a transverse serial section that shows the small medial fin fold as a fold in the epidermal ectoderm. The large somites are lateral to the spinal cord and notochord. The caudal artery (CA) and caudal vein (CV) are located dorsal to the small gut (G) (200x, PS).

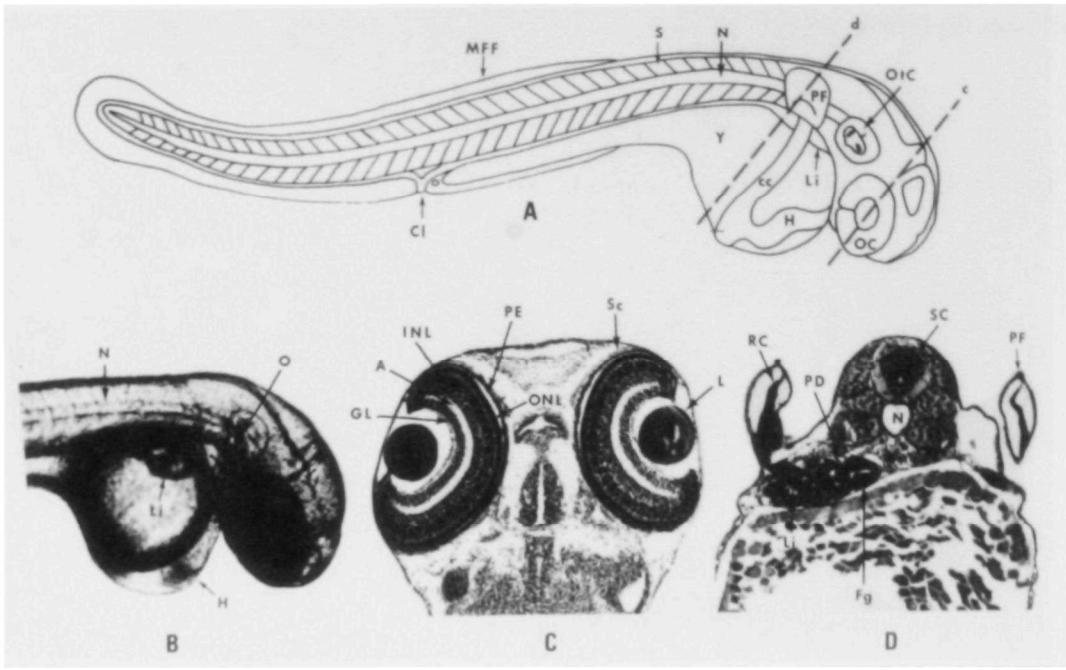

Stage 28: Blood in pectoral fins. **Plate 28**

Blood flows through a single loop in the pectoral fins (PF). Dark stellate melanocytes are present on the ventral surface of the yolk sac (Y) anterior to the cloaca (Cl). An enlarged vessel dorsal to the myotomes receives blood from the segmental arteries. The six aortic arches branch off of the ventral aorta. Ventral and lateral evaginations into the lumen of the otic capsule (OtC) have appeared. The liver (Li) has noticeably enlarged. The thick-walled heart (H) lies completely on the yolk sac (Y). The angle of the cephalic flexure has decreased. The hyaline sheath surrounding the notochord (N) has thickened. The banding pattern of the skeletal muscle is more apparent.

Cranial ganglia V, IX, and X have connected with the diencephalon and myelencephalon. A bridge of tissue representing the semicircular canal anlage is visible in the otic capsules. Neuromasts continue to proliferate throughout the head region. The olfactory grooves have sent out axons which link up with the olfactory lobes of the telencephalon. The operculum extends caudally from the hyoid arch and covers branchial arches 3, 4, and 5. White matter extends along the dorsal and lateral sides of the spinal cord for most of its length.

The optic cup (OC) has darkened considerably, obscuring much of the lens. The eyes are enclosed in a 2-3 cell-thick layer of undifferentiated mesoderm, the early sclerotic coat (SC) which is enclosed the by the pigment epithelium (PE). The retina itself has differentiated into a layer of columnar cone precursor cells, a bipolar layer, and the thick ganglion cell layer (GL). The distinctive choroid fissure pierces all layers of the eye, and is the route of exit for the optic nerve and entry for the hyoid artery. The thin layer of epidermal ectoderm and mesoderm covering the eye has not yet differentiated into cornea.

The hindgut makes an abrupt ventral turn above the cloacal opening, then increases in size just prior to merging with the opening of the urinary bladder anlage. Paired posterior pronephric ducts (PD) join into a single enlarged duct lined with columnar epithelium, the urinary bladder anlage, which also makes an abrupt ventral turn prior to merging with the small cloaca. Paired pronephric ducts extend anteriorly

to the pectoral fins. Cartilaginous tissue is differentiating in the upper and lower jaws. The pharynx is large and triangular anteriorly, becoming compressed dorsally and ventrally prior to merging with the foregut (Fg). A bend in the foregut is visible under the pectoral fins. Radial cartilage (RC) is forming in the pectoral fins.

Figure A is a line drawing that shows the cloaca which functions as the common exit for the digestive and urinary system. The otic capsule, liver, somites (S), and heart (H) continue to differentiate. A small vessel loops through the pectoral fin with a visible blood flow. The planes of section for Figures C and D are indicated by dashed lines (c) and (d), respectively (80x, LD). In Figure B the liver is visible extending into the yolk sac of living embryos. The optic cups appear as dark masses due to extensive pigmentation. Note the thickened walls of the otic capsule (80x, LS). Figure C is an oblique serial section that shows the lens and layers of the eye, the sclerotic coat, the pigment epithelium, the outer nuclear layer (ONL), the inner nuclear layer (INL), internal plexiform layer, and the ganglion cell layer (200x, PS). Figure D is a transverse section that shows the radial cartilage in the pectoral fin. The thick-walled foregut is medial to the liver tissue. Paired pronephric ducts are ventral and lateral to the notochord (200x, PS).

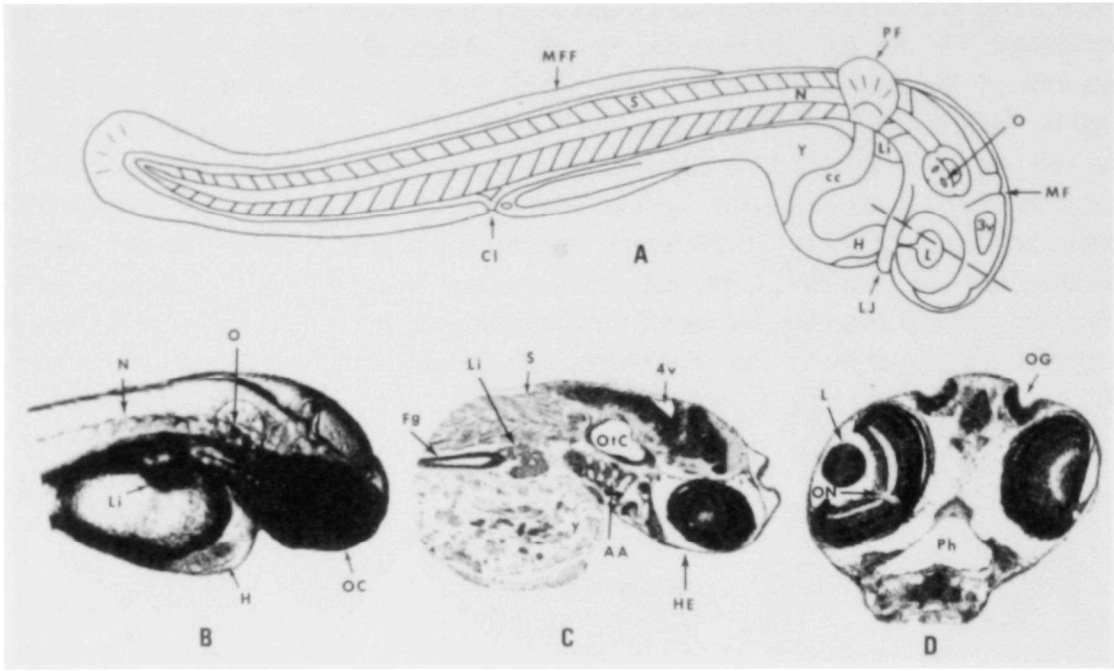

Stage 29: Bile formation. **Plate 29**

Further differentiation has occurred in the cartilage of the jaw apparatus. Limited movement of the lower jaw and eyes in living embryos is first seen at this stage. Yellowish bile in the gall bladder has formed and is visible in living embryos. A dip is present in the median fin fold (MFF) around the cloacal (Cl) opening. The number of stellate melanocytes has increased on the ventral yolk sac (Y). The caudal artery has replaced the posterior dead-end vessel of the previous stage. Striated muscle and basal cartilage is present in the base of the pectoral fins (PF0). The ampullae anlagen at the base of the semicircular canal are visible as thickenings in the walls of the otic capsule (OtC). The foregut (Fg) has differentiated into a thick-walled stomach with an enlarged lumen. Blood flow can now be observed in the liver (Li) sinusoids. The olfactory grooves (OG) are bordered internally by a squamous cell layer, and externally by a lighter-staining sensory layer.

Figure A is a line drawing that illustrates the lower jaws (LJ) and the continued differentiation of the otic capsule. Also visible are the notochord (N), heart (H), common cardinal veins (CC), third (3v) and fourth (4v) ventricle, choroid fissure, somites (S), and median fin fold. The plane of section of Figure D is indicated by the dashed line (80x, LD). In Figure B the otic capsule and the highly pigmented optic cup (OC) are seen (80x, LS). Also note the heart on the anterior aspect of the yolk mass. Figure C is a sagittal serial section that shows the thick-walled foregut and liver tissue. Four aortic arches (AA) are visible in the branchial arches (80x, PS). Figure D is an oblique serial section that shows the optic nerve in the optic cup. The large olfactory groove, head ectoderm (HE), and pharynx (Ph) are also visible (100x, PS).

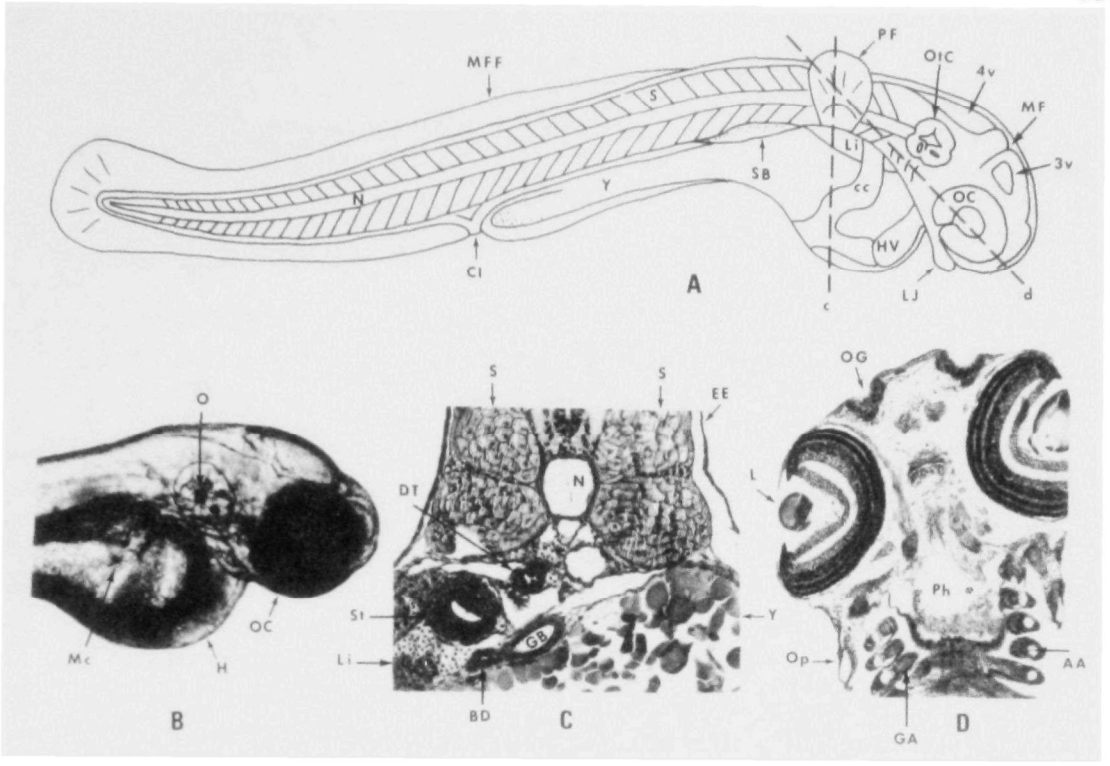

Stage 30: Swim bladder. **Plate 30**

At this stage embryos hatch out of the chorion if disturbed by handling or bright lights. The swim bladder (SB) which appeared at 90 hr (at 25°C) has enlarged and is pigmented dorsally. It maintains its connection with the foregut through a thin hollow cord of cells. The stomach (St) is thick-walled and is developing internal folds. The lumen of the gall bladder (GB) is lined with a single layer of columnar cells, and is connected to the intestine by a short bile duct. The yellow bile from the bile duct (BD) is visible, extending caudally into the intestine.

The eyes, jaws, pectoral fins (PF), and operculum (Op) exhibit frequent movements. The mandibular adductor and levator muscles have formed in the head region in association with the protruding lower jaw (LJ). The mouth is now open. The epidermal ectoderm (EE) covering the shrinking yolk sac (Y) has a wrinkled appearance. The somites (S) extend to the posterior edge of the otic capsule (OtC). Increased pigmentation is visible on the ventral yolk sac. Melanocytes are present at intervals along the lateral line system associated with the neuromasts. The number of striations in the caudal fin is increasing. A series of evaginations representing the gill anlagen are visible on the posterior surface of gill arches (GA). The operculum (Op) has enlarged and covers all four gill arches.

In Figure A the dorsally pigmented swim bladder is illustrated caudal to the liver (Li). The ventricle of the heart (HV) is large and thick-walled. Note the location and differentiation of the otic capsule, third (3v) and fourth (4v) ventricle, meten-mesencephalic fissure (MF), and median fin fold (MFF). The planes of section for Figures C and D are indicated by dashed lines (c) and (d), respectively (80x, LD). In Figure B the large paired otoliths (O) are visible in the otic capsule. Stellate melanocytes (Mc) are visible on the yolk sac. The optic cups (OC) appear as heavily pigmented masses in the head region (80x, LS). In Figure C the dorsal tube (DT) that connects the thick-walled stomach to the swim bladder is visible ventral to the notochord (N). The gall bladder and bile duct are visible medial to the liver tissue. The large somites (S) are bounded by the layer of epidermal ectoderm (200x, PS). In Figure D the

operculum can be seen lateral to the aortic arches in the gill arches. Note the presence of olfactory grooves medial to the optic cups and the centrally located pharynx (Ph) (100x, PS).

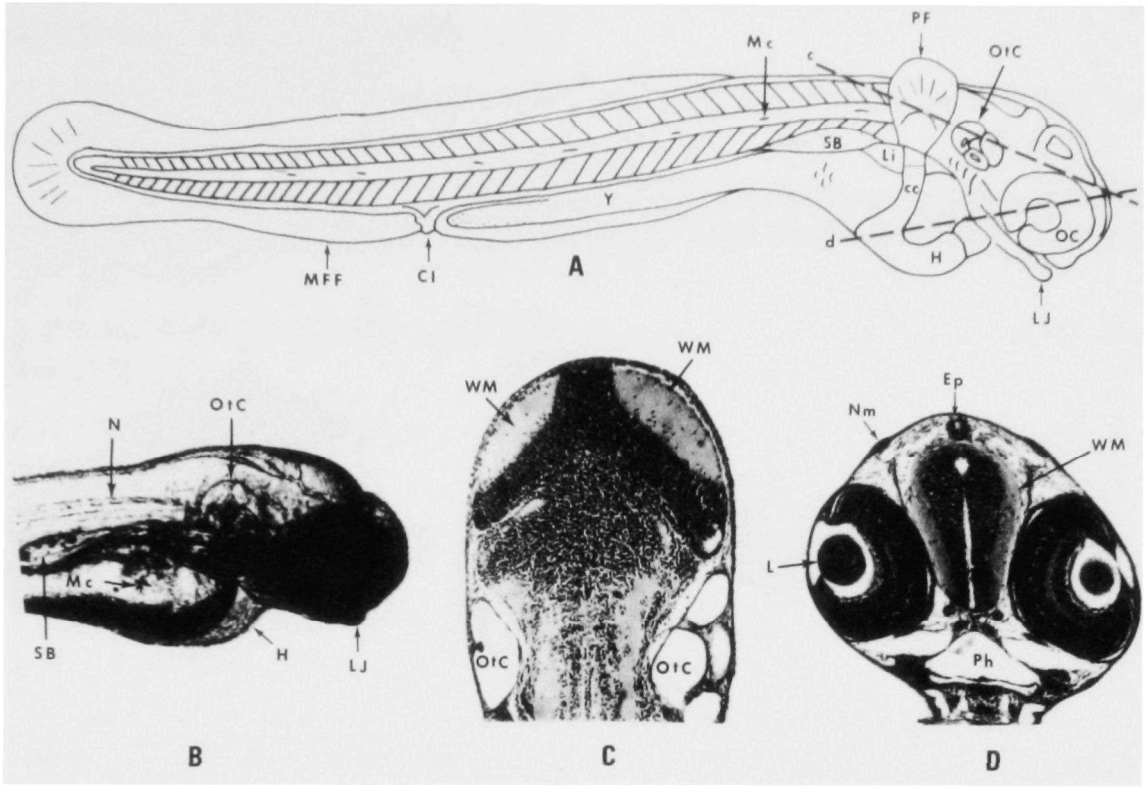

Stage 31: Large operculum. **Plate 31**

Under control conditions (at 25°C) a few fish hatch out of the chorion at this stage. Blood flow in the aortic arches has increased. The gill anlagen have enlarged. The operculum covers the otic capsule (OtC). The lower jaw (LJ) is well-formed. Striations are prominent in the caudal and pectoral fins (PF). Pigment cells continue to migrate anteriorly on the ventral yolk sac (Y). The swim bladder (SB) has increased in size and pigmentation, and maintains its attachment to the gut by a small dorsal tube. The intestine has become pigmented. Bile production has increased, as indicated by large areas of yellow pigment in the gall bladder and intestine.

Figure A is a line drawing that gives the overall appearance of the embryo. Note that the swim bladder and liver continue to enlarge. Planes of section of Figures C and D are indicated by dashed lines (c) and (d), respectively (80x, LD). Figure B shows how the embryo has become more streamlined in appearance due to a decrease in size of the yolk sac and a straightening of the embryonic axis. Note the large notochord (N), the blood filled heart (H), swim bladder, and melanocytes (Mc) (80x, LS). In Figure C white matter is seen on the lateral aspects of the tectal lobes anterior to the otic capsule (200x, PS). Figure D is a transverse serial section that shows the epiphysis (Ep) dorsal to the diencephalon. The lateral aspects of the diencephalon are covered with white matter. Lens-shaped neuromeres (Nm) are visible associated with the epidermal ectoderm. The triangular pharynx (Ph) is also visible in this section (200x, PS).

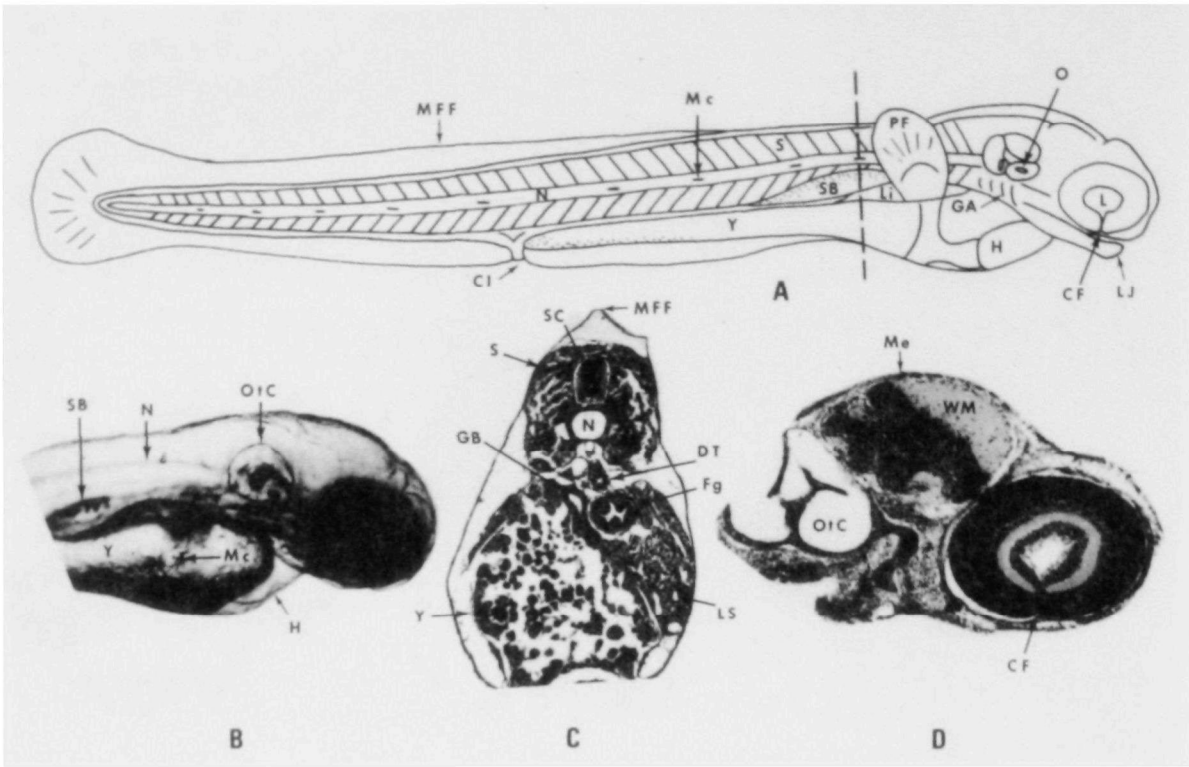

Stage 32: Gill anlagen, hatching. **Plate 32**

The majority of the embryos have hatched out of the chorion at this stage. The operculum and lower jaw (LJ) are well-formed and move often. The superior, lateral, and medial rectus muscles are visible in serial sections and result in frequent eye movement. The yolk sac (Y) is much reduced and has become more streamlined in shape. A strong blood flow is present through the gill anlagen. The lumen of the stomach has enlarged, and thickenings in its walls are visible histologically in both anterior and posterior regions. Blood flow in the liver sinusoids (LS) has increased. A large neuromast is visible laterally on each operculum. The pronephric ducts are adjacent to the cardinal veins on their lateral ventral surface, although no glomeruli are present.

Figure A is a composite line drawing that illustrates the reduced yolk sac, as well as the medial fin fold (MFF), melanocytes (Mc), cloaca (Cl), somites (S), swim bladder (SB), liver (Li), pectoral fins (PF), gill arches (GA), otoliths (O) in the otic capsule (OtC), heart (H), choroid fissure (CF), lens (L) and lower jaw. Plane of section of Figure C is indicated by the dashed line (80x, LD). In Figure B the notochord is visible extending up to the posterior edge of the distinctive optic cup. Stellate melanocytes continue to migrate over the yolk sac (80x, LS). Figure C is a transverse serial section that shows the gall bladder (GB) and the dorsal tube (DT) that connects the foregut (Fg) with the swim bladder. The liver sinusoids appear as clear spaces in the liver tissue. Note the presence of the spinal cord (SC) and the lateral somites (S) (200x, PS). Figure D is a sagittal serial section that shows the large otic capsule and white matter (WM) of the mesencephalon (Me), as well as the ventral choroid fissure in the optic cup (200x, PS).

REFERENCES

Allen, A.L. and Mulkay, L.M. (1960). X-ray effects on embryos of the paradise fish, with notes on normal stages. Growth 24, 131-168.

Andrews, A.K. (1970). Life history of the fathead minnow. Ph.D. dissertation, Colorado State University. 131 pp.

Andrews, A.K. and Flickinger, S.A. (1974). Spawning requirements and characteristics of the fathead minnow. Proceedings of the 27th Annual Conference, S.E. Assoc. Game and Fish Comms., 759-766.

Armstrong, P.B. and Child, J.S. (1965). Stages in the normal development of Fundulus heteroclitus. Biol. Bull., 128, 143-168.

Ballard, W.W. (1966). Origin of the hypoblast in Salmo I. Does the blastodisc edge turn inward? J. Exp. Zool., 161, 201-210.

Ballard, W.W. (1973). Normal embryonic stages for salmonid fishes based on Salmo gairdneri (Richardson) and Salvelinus fontinalis (Mitchell). J. Exp. Zool., 184, 7-26.

Ballard, W.W. and Needham, R.G. (1964). Normal embryonic stages of Polyodon spathula (Walbaum). J. Morph., 114, 465-473.

Battle, H.I. (1944). The embryology of the Atlantic salmon (Salmo salar Linnaeus). Can. Jour. Re search, 22(D), 105-125.

Benoit, D.A. and Carlson, R.W. (1977). Spawning success of fathead minnows on selected artificial substrates. Prog. Fish. Cult., 39, 67-69.

Breder, C.M., Jr. (1922). Some embryonic and larval stages of the winter flounder. Bull. U.S. Bur. Fish., 38, 311-316.

Bullough, W.S. (1939). A study of the reproductive cycle of the minnow in relation to the environment. J. Zool. Proc. Zool. Soc. London, 109, 79-102.

Coombs, H.S. and Hiby, A.R. (1979). The development of the eggs and early larvae of blue whiting, Micromesistius poutassou, and the effect of temperature on development. J. Fish. Biol., 14, 111-123.

Denny, J.S. (1987). Guidelines for the culture of fathead minnows, Pimephales promelas, for use in toxicity tests. EPA 600-387-001. U.S. Environmental Protection Agency, Duluth, MN.

Deuel, D.G., Clark, J.R. and Mansueti, A.J. (1966). Description of embryonic and early larval stages of bluefish, Pomatomus saltatrix. Trans. Amer. Fish. Soc., 95, 264-271.

Devlin, E.W. (1982). Acute toxicity of toluene to three age groups of fathead minnows (Pimephales promelas). Bull. Environm. Contam. Toxicol., 29, 12-17.

El Zarka, S. and Ezzat, A. (1972). Embryology and larval development of Talapis galilae Art. Rapp. Comm. Ent. Mer. Medit., 20, 499-501.

Galat, D.L. (1973). Normal embryonic development of the muskellunge (Esox masquinongy). Trans. Amer. Fish. Soc., 102, 384-391.

Harrington, W.R. (1947). The early life history of the bridled shiner, Notropis bifrenatus (Cope). Copeia, 1947, 97-102.

Hisaoka, K.K. and Battle, H.I. (1958). The normal development stages of the zebrafish, Brachydanio-rerio (Hamilton-Buchanan). J. Morphol., 102, 311-328.

Hodges, W.R. and Behre, E.H. (1953). Breeding behavior, early embryology, and melanophore development in the anabantid fish, Trichogaster trichopterus. Copeia, 1953, 101-107.

Humason, G.L. (1979). Animal Tissue Techniques. W.H. Freeman and Co., San Francisco, p.21.

Kajishima, T. (1960). The normal developmental stages of the goldfish Carassius auratus. Jap. Jour. Ichth., 8, 20-28.

Kirchen, V.K. and West, W.R. (1976). The Japanese medaka, its care and development. Carolina Biological Supply Company, Burlington, NC. 36pp.

Koenig, C.C. and Livingston, R.J. (1976). The embryonic development of diamond killifish, Adinia xenica. Copeia, 1976, 435-444.

Long, L.W. and Ballard, W.W. (1976). Normal embryonic stages of the white sucker, Catostomus commersoni. Copeia, 1976(2),342-351.

Lord, R.F., Jr. (1927). Notes on the use of the blackhead minnow, Pimephales promelas, as a forage fish. Trans. Amer. Fish. Soc., 57, 92-94.

Lund, A.W. and March, B.C. (1975). Early development of the grubby, Myoxocephalus aenaeus. Biol. Bull., 149, 373-383.

Mahon, E.E. and Hoar J.R. (1956). The early development of the chum salmon, Oncorhynchus keta (Walbaum). J. Morphol., 98, 1-48.

Mansueti, A.J. (1964). Early development of the yellow perch, Perca flavescens. Ches. Sci., 5(1-2), 46-66.

Manner, W.J. and Dewese, C.M. (1974). Early embryology of the fathead minnow. Anat. Rec., 180, 99-110.

Markaus, H.C. (1934). Life history of the bullhead minnow (Pimephales promelas). Copeia, 1934, 116-122.

McClendon, J.F. (1912). Effect of alkaloids on the development of fish (Fundulus) eggs. Amer. J. Physiol., 31, 131-140.

McKim, J.M. (1977). Evaluation of tests with early life stages of fish for predicting long-term toxicity. J. Fish. Res.Board Can., 34, 1148-1154.

Niazi, A.D. (1963). The development of the weberian system and early embryology of Pimephales promelas. Ph.D. Thesis, Oklahoma State University, Stillwater, Okla. 126pp.

Penaz, M. (1973). Embryonic development of the barb, Barbus barbus. Zool. Listy., 22, 363-374.

Price, J.W. (1934a). The embryology of the whitefish, Coregonus clupeaformis. (Mitchill). Part I. Ohio J. Sci., 34, 399-414.

Price, J.W. (1934b). The embryology of the whitefish, Coregonus clupeaformis (Mitchill). Part II. Ohio J. Sci., 34, 399-414.

Price, J.W. (1935). The embryology of the whitefish, Coregonus clupeaformis (Mitchill). Part III. Ohio J. Sci., 35, 40-53.

Saksena, V.P., Yamamoto, K. and Riggs, C.D. (1961). Early development of the channel catfish. Progr. Fish Cult., 23, 156-161.

Shaklee, J.B., Champion, M.J. and Whitt, G.S. (1974). Developmental genetics of teleosts; A biochemi cal analysis of lake chubsucker ontogeny. Dev. Biol., 38, 356-382.

Shaw, E.S. (1955). The embryology of the sargent major, Abudefduf saxatilis. Copeia, 55, 85-89.

Stockard, C.R. (1910). The influence of alcohol and other anaesthetics on embryonic development. Amer. J. Anat., 10, 369-392.

Thakur, N.K., Pal, R.N. and Khan, H.A. (1974). Embryonic and larval development of Heteropneustes fossilis (Bloch). J. Inland Fish. Soc. India, 6, 33-44.

Till, J.E. (1977). Laboratory technique for obtaining fathead minnow eggs for use in toxicity experiments. Progressive Fish. Cult., 39, 24-27.

Velsen, F.P.J. (1980). Embryonic development in eggs of sockeye salmon, Oncorhynchus nerka. Can. Special Pub. Fish Aquatic Sci., 49, 19p.

Vrat, V. (1949). Reproductive behavior and development of eggs of the three-spined stickleback (Gasterosteus aculeatus) of California. Copeia, 1949, 252-260.

Wabuke-Bunoti, M.A.N. (1980). Thyroid gland development in the prehatching fathead minnow, Pimephales promelas, Rafinesque. MS dissertation, University of Minnesota-Duluth. 131 pp.

Wallace, C.R. (1972). Embryonic and larval development of the small mouth bass at 23 C. Prog. Fish. Cult., 34,2 37-234.

Wilson, H.V. (1891). Embryology of the sea bass (Serranus atratius). Bull. U.S. Fish. Comm., 9, 209-277.

Wourms, J.P. (1972). Developmental biology of annual fishes I. Stages in the normal development of Austrofundulus myersi Dahl. J. Exp. Zool., 182, 143-153.

Zeitoun, I.H. (1974). The embryology of the coho salmon. Trans. Amer. Fish. Soc., 103, 371-375.